Spring 3-1-1988

Planar Analysis and Optimization of Microstrip Discontinuities

Henri J. Maramis
University of Colorado Boulder

K C. Gupta
University of Colorado Boulder

Scientific Report No. 96

Planar Analysis and Optimization of Microstrip Discontinuities

Henri J. Maramis
K. C. Gupta

Electromagnetics Laboratory
Department of Electrical and Computer Engineering
University of Colorado
Boulder, CO 80309-0425

March 1988

Work reported in this report has been supported by TRW Inc. Electronics System Group through their Research Contract No. TRWE881582T65.

Abstract

This report discusses planar analysis of microstrip discontinuities using segmentation and/or desegmentation method. Computer program for implementation of planar analysis is discussed. The numerical results obtained by planar analysis are compared with results obtained by quasi-static analysis and by full-wave spectral domain analysis. Also, the planar analysis is used for optimization of microstrip discontinuities; and the results are compared with experimental results given by Hammerstad.

Contents

List of Figures

List of Tables

Chapter 1

Introduction

An accurate and reliable characterization of microwave/millimeter-wave circuit components is one of the basic prerequisites of a successful CAD. The degree of accuracy to which the performance of microwave/millimeter-wave integrated circuits can be simulated depends upon the accuracy of the characterization and modelling of components. Inadequacy of the modelling of junctions and discontinuities in transmission structures has been recognized as one of the key bottle-necks in microwave/millimeter-wave CAD.

Various methods available for characterization of microstrip discontinuities may be divided into three groups:

- 1. Quasi-static techniques for evaluation of capacitances and inductances associated with various discontinuity configurations.
- 2. Planar model analysis leading to frequency dependent scattering matrix evaluation of discontinuities like steps, bends, tee-junctions, cross-junctions, etc.
- 3. Full-wave analysis techniques using spectral domain and/or moment method or finite-element analysis or TLM approaches.

This report discusses the planar analysis of microstrip discontinuities using segmentation/desegmentation method (see [1], [2], [3], [4], [5], [6], [7]). Planar analysis of microstrip discontinuities is based on the parallel-plate waveguide planar model of the microstrip line fields. Planar analysis of microstrip lines and discontinuities gives more accurate results than quasi-static analysis does, and it is simpler than the rigorous full-wave analysis. Before

the discussion of segmentation/desegmentation methods, the planar waveguide models of microstrip line and microstrip discontinuities are presented. The computer code developed for planar analysis of microstrip discontinuities, the convergence of the results and the shift of reference planes are discussed in the Section on implementation. The numerical results are compared with quasi-static analysis and spectral domain analysis results. The use of planar analysis using segmentation/desegmentation method for optimization of microstrip discontinuities is discussed and some comparisons of the numerical results are presented. Finally, the conclusion and the plan for future work are discussed in the last Chapter.

Chapter 2

Planar Waveguide Model of Microstrip Line

In this Chapter, the planar waveguide model of microstrip line is discussed (see [5], [8], [9], [10]). The frequency dependent quantities such as the effective width, characteristic impedance, effective dielectric constant, and losses are discussed first. The last Section describes the modelling of microstrip discontinuities using the planar waveguide model of microstrip line.

2.1 The effective width of planar waveguide model

The planar waveguide model of microstrip line is shown in Figure 2.1. The ideal planar waveguide consists of two parallel conductors bounded by magnetic walls (i.e. no normal component of the electric field, nor tangential component of the magnetic field) in the transverse directions. The electric and magnetic fields in the dielectric region are uniform because there are no fringing fields outside the magnetic walls (see Figure 2.1(b)).

The width of the model is larger than the physical width in order to account for the fringing/edge fields of microstrip. This width is called the effective width $w_e(f)$. The effective width is determined from the characteristic impedance $Z_0(f)$ and the effective dielectric constant $\epsilon_{r_e}(f)$ according to the parallel plate waveguide formula:

$$w_e(f) = \frac{\eta_0 h}{Z_0(f)\sqrt{\epsilon_{r_e}(f)}} \tag{2.1}$$

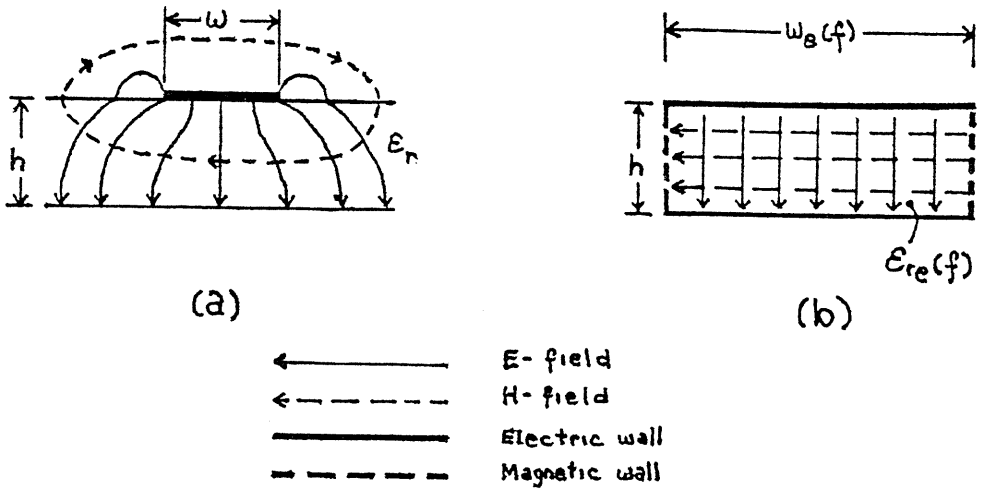

Figure 2.1: Planar waveguide model for microstrip line: (a) original circuit; (b) planar model.

where η_0 is the wave impedance in air/vacuum ($= 120\pi\Omega$); h is the substrate height; $Z_0(f)$ is the dynamic characteristic impedance; and $\epsilon_{r_e}(f)$ is the dynamic effective dielectric constant.

2.2 Characteristic impedance and effective dielectric constant

An accurate closed-form expression for characteristic impedance and effective dielectric constant has been reported by Hammerstad and Jensen [11]. The expressions for $Z_0(\frac{w}{h}, t = 0)$ in a homogeneous media ($\epsilon_r = 1$) and for $\epsilon_{r_e}(\frac{w}{h}, \epsilon_r, t = 0)$ are derived from functional approximation of analytical equations for t (the strip thickness) equal to zero. The expression for $Z_0(\frac{w}{h}, t = 0)$ for $\epsilon_r = 1$ based on [11] is given below:

$$Z_0(\frac{w}{h}, t = 0) = \frac{\eta_0}{2\pi} ln(\frac{f(\frac{w}{h})}{\frac{w}{h}} + \sqrt{1 + (\frac{2h}{w})^2}) \tag{2.2}$$

where,

$$f(\frac{w}{h}) = 6 + (2\pi - 6)exp(-(30.666\frac{h}{w})^{0.7528}) \tag{2.3}$$

This expression valid for $0 < \frac{w}{h} < \infty$. The maximum error of Equation (2.2) is 0.01% for $\frac{w}{h} < 1$ and 0.03% for $\frac{w}{h} < 1000$ compared to the exact solutions.

The expression for $\epsilon_{r_e}(\frac{w}{h}, \epsilon_r, t = 0)$ given by [11] is an extension of the Schneider's equation [12]:

$$\epsilon_{r_e}(\frac{w}{h}, \epsilon_r, t = 0) = \frac{\epsilon_r + 1}{2} + \frac{\epsilon_r - 1}{2}(1 + \frac{10h}{w})^{-a(\frac{w}{h})b(\epsilon_r)} \tag{2.4}$$

where,

$$a(\frac{w}{h}) = 1 + \frac{1}{49}ln(\frac{(\frac{w}{h})^4 + (\frac{w}{52h})^2}{(\frac{w}{h})^4 + 0.432}) + \frac{1}{18.7}ln(1 + (\frac{w}{18.1h})^3) \tag{2.5}$$

$$b(\epsilon_r) = 0.564(\frac{\epsilon_r - 0.9}{\epsilon_r + 3})^{0.053} \tag{2.6}$$

The accuracy of this expression is better than 0.2% for $0.01 < \frac{w}{h} < 100$ and $1 \leq \epsilon_r \leq 128$.

2.2.1 Expressions for Z_0 and ϵ_{r_e} taking into account the effect of finite conductor thickness of microstrip

The expression for $Z_0(\frac{w}{h}, \frac{t}{h}, \epsilon_r)$ and $\epsilon_{r_e}(\frac{w}{h}, \frac{t}{h}, \epsilon_r)$ are derived by Hammerstad and Jensen [11] from a functional approximation of the numerical results for conductor thickness $t > 0$ and conductor width $w_e = w + \Delta w$ (w_e not to be confused with $w_e(f)$ in Equation (2.1)). The resulting expressions are very accurate for narrow strip and for substrates with low dielectric constant. For homogeneous media ($\epsilon_r = 1$) the width correction is [11]:

$$\Delta w_{t,0} = \frac{t}{\pi}ln(1 + \frac{4exp(1)}{(\frac{t}{h})coth^2(\sqrt{6.517\frac{w}{h}})}) \tag{2.7}$$

where $exp(1) = e = 2.71828$ (base of the natural logarithm); and $w_{e,0} = w + \Delta w_{t,0}$ is the corrected strip width for $\epsilon_r = 1$. For $\epsilon_r > 1$, the width correction is [11]:

$$\Delta w_t = \frac{\Delta w_{t,0}}{2}(1 + \frac{1}{cosh(\sqrt{\epsilon_r - 1})}) \tag{2.8}$$

where $w_e = w + \Delta w_t$ is the corrected width for $\epsilon_r > 1$. Thus, using Equations (2.7) and (2.8) the effect of strip thickness can be included in the computations of Z_0 and ϵ_{r_e} [11] as follow:

$$\begin{aligned} Z_0(\frac{w}{h}, \frac{t}{h}, \epsilon_r) &= Z_0(\frac{w_e}{h}, t = 0, \epsilon_r) \\ &= \frac{Z_0(\frac{w_e}{h}, t = 0)}{\sqrt{\epsilon_{r_e}(\frac{w_e}{h}, t = 0, \epsilon_r)}} \end{aligned} \tag{2.9}$$

and

$$\begin{aligned} \epsilon_{r_e}(\frac{w}{h}, \frac{t}{h}, \epsilon_r) &= (\frac{Z_0(\frac{w_{e,0}}{h}, t = 0)}{Z_0(\frac{w_e}{h}, t = 0, \epsilon_r)})^2 \\ &= \epsilon_{r_e}(\frac{w_e}{h}, t = 0, \epsilon_r)(\frac{Z_0(\frac{w_{e,0}}{h}, t = 0)}{Z_0(\frac{w_e}{h}, t = 0)})^2 \end{aligned} \tag{2.10}$$

where $Z_0(\frac{w_e}{h}, t = 0)$ and $Z_0(\frac{w_{e,0}}{h}, t = 0)$ are given by Equation (2.2); and $\epsilon_{r_e}(\frac{w_e}{h}, t = 0, \epsilon_r)$ is given by Equation (2.4).

2.2.2 Expressions for Z_0 and ϵ_{r_e} taking into account the effect of dispersion in microstrip

Both characteristic impedance and effective dielectric constant vary with frequency because microstrip propagation is not purely TEM. Getsinger [13] used the Longitudinal-Section Electric (LSE) mode dispersion model to account for the dispersion in the effective dielectric constant. The model consists of a wave medium that allows LSE modes to propagate (see Figure 2.2). The wave conductor model is defined by electric and magnetic walls. Since the field distribution in the model is different than in the original circuit hence, the dispersion model does not have exactly the same dispersion function $\epsilon_{r_e}(f)$ as the original circuit. A good approximation can be achieved because the fields in microstrip are concentrated below the parallel plate capacitor section and in the conductor edges (fringing fields). Near the conductor edges the electric field is parallel and the magnetic field is perpendicular to the dielectric boundary. Thus, the model is divided into three regions (see Figure 2.2(b)).

Region I is a planar waveguide with dielectric constant ϵ_r (the same ϵ_r as the substrate of the original circuit) and an arbitrarily chosen plate separation

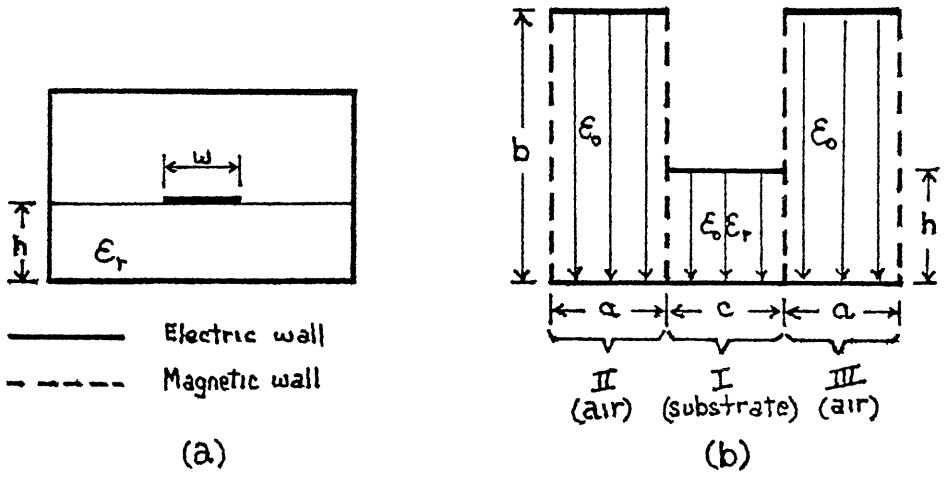

Figure 2.2: LSE dispersion model: (a) original circuit; (b) LSE dispersion model.

h which generates the parallel plate capacitor field. The other regions, II and III, represent the fields in air of the original configuration. The planar waveguides of regions II and III have larger plate separation because the air-filled section is larger than the substrate. The E-field lines are parallel and the H-field lines are perpendicular to the dielectric boundary in the model. The dispersion of the model is adjusted to be the same as the dispersion of the original circuit by choosing the right values of b/a, c/h and b/h. The right choice of b/a and c/h will match the values of $Z_0(\frac{w}{h}, \frac{t}{h}, \epsilon_r)$ and $\epsilon_{r_e}(\frac{w}{h}, \frac{t}{h}, \epsilon_r)$ of the model to the original circuit. Thus, the dispersion function $\epsilon_{r_e}(f)$ of the model is determined by the transverse resonance method [14]. If the result matches the numerically determined dispersion function of the original circuit then the value b/h can be determined. The resulting dispersion function is [13]:

$$\epsilon_{r_e}(f) = \epsilon_r - \frac{\epsilon_r - \epsilon_{r_e}(\frac{w}{h}, \frac{t}{h}, \epsilon_r)}{1 + G(\frac{f}{f_p})^2} \tag{2.11}$$

where f is the operating frequency and $f_p = Z_0(\frac{w}{h}, \frac{t}{h}, \epsilon_r)/(2\mu_0 h)$ is an approximation to the first TE-mode cut-off frequency. G is a dimensionless factor which is empirically determined. The expression for G by [13] fits experimental data for alumina substrate only. Hammerstad and Jensen [11]

gave an expression for G for any types of substrate now in use:

$$G = \frac{\pi^2}{12} \frac{\epsilon_r - 1}{\epsilon_{r_e}(\frac{w}{h}, \frac{t}{h}, \epsilon_r)} \sqrt{\frac{2\pi Z_0(\frac{w}{h}, \frac{t}{h}, \epsilon_r)}{\eta_0}} \tag{2.12}$$

Based on the parallel-plate model and the theory of dielectric the characteristic impedance can be expressed as follows [11]:

$$Z_0(f) = Z_0(\frac{w}{h}, \frac{t}{h}, \epsilon_r) \sqrt{\frac{\epsilon_{r_e}(\frac{w}{h}, \frac{t}{h}, \epsilon_r)}{\epsilon_{r_e}(f)}} \frac{\epsilon_{r_e}(f) - 1}{\epsilon_{r_e}(\frac{w}{h}, \frac{t}{h}, \epsilon_r) - 1} \tag{2.13}$$

where $Z_0(\frac{w}{h}, \frac{t}{h}, \epsilon_r)$ is given by Equation (2.9) and $\epsilon_{r_e}(\frac{w}{h}, \frac{t}{h}, \epsilon_r)$ is given by Equation (2.10). These last two equations for Z_0 and ϵ_{r_e} (Equations (2.11) and (2.13)) are used in computing the effective width of the microstrip as given in Equation (2.1).

2.3 Losses in microstrip line

The conductor loss is computed [5] by assuming that a very small electric field (small enough not to disturb the field configuration) exists on the surface of the conductors. Thus, the Poynting vector has a small component normal to the conductors. The attenuation constant is derived from the power attenuation rate, knowing the surface impedance of a metallic material when the conductivity σ is much larger than $(\omega\epsilon)$. Hence, the attenuation constant due to conductor loss can be expressed as [5]:

$$\alpha_c = \omega\sqrt{\mu\epsilon}\frac{r}{2h} \tag{2.14}$$

where h is the plate separation and $r = \sqrt{\frac{2}{\omega\mu\sigma}}$ is the skin depth of the conductor.

Similarly, the dielectric loss is derived from the power attenuation rate due to dielectric loss [5]. The expression for the attenuation constant due to the dielectric loss is given below:

$$\alpha_d = \omega\sqrt{\mu\epsilon}\frac{\tan\delta}{2} \tag{2.15}$$

where $\tan\delta$ is the loss tangent delta of the dielectric.

Comparing Equations (2.14) and (2.15), one can define an equivalent loss tangent delta to account for the conductor loss as:

$$\tan \delta_c = \frac{1}{h\sqrt{\mu \pi f \sigma}} \tag{2.16}$$

Thus, the effective loss tangent of the dielectric (including the conductor loss) can be expressed as:

$$\begin{aligned} \tan \delta_e &= \tan \delta + \tan \delta_c \\ &= \tan \delta + \frac{1}{h\sqrt{\mu \pi f \sigma}} \end{aligned} \tag{2.17}$$

where $\mu = \mu_0$ is the free space permeability; f is the operating frequency; and σ is the conductivity of the metallic material.

2.4 Planar waveguide model of microstrip discontinuities

Planar waveguide models of microstrip discontinuities can be derived from the planar waveguide model of microstrip line. The planar waveguide models of four microstrip discontinuities are illustrated in Figure 2.3.

In all of these cases, the straight section of microstrip lines are modelled using the planar waveguide model of microstrip line with their effective widths, effective dielectric constants, and effective loss tangent computed using Equations (2.1), (2.11), and (2.17) respectively. The discontinuity region is modelled by extrapolating the effective dimensions. In Figure 2.3(a), the outer corner (between planes $T - T$) is obtained by extending the outer dimensions to meet at *oc*. In Figure 2.3(b), the poins x and y, which are obtained by replacing w by $w_e(f)$, are joint together. In Figure 2.3(c), the junction planes $T - T$ is shifted towards the narrower line by an amount Δl (obtained from the open-end capacitance of microstrip of width w). In Figure 2.3(d), the planar model of the tee-junction is obtained by extending the effective boundary as shown.

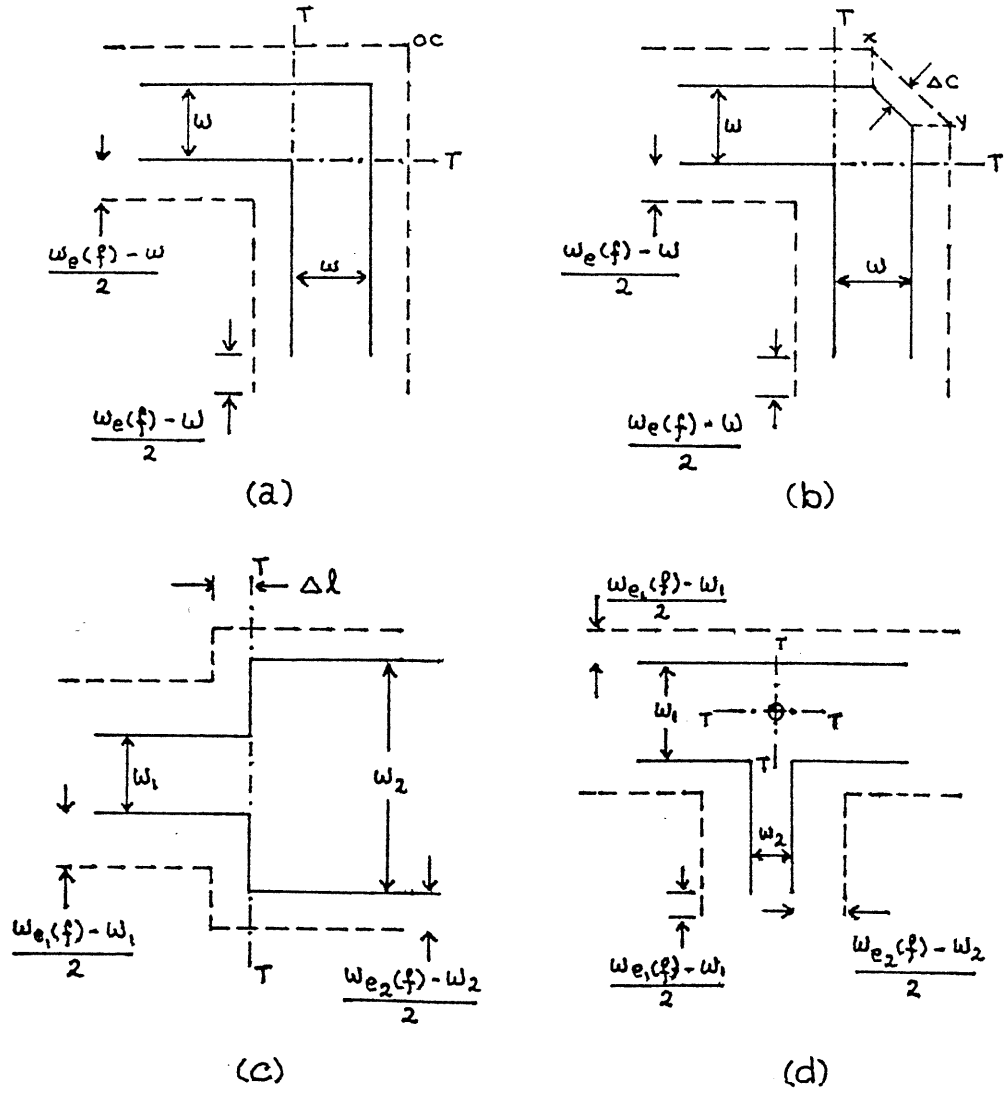

Figure 2.3: Planar waveguide models of four microstrip discontinuities: (a) right-angle bend; (b) chamfered right-angle bend; (c) step-in-width; (d) tee-junction.

Chapter 3

Analysis of Planar Structures

Three methods of analyzing the planar structures will be presented in this Chapter. The first one is the Green's function approach which is used if the structure is made up of a single regular segment only. The second method is the segmentation method which is used when the structure is a composite of several regular segments for which the Green's functions are available. The third method is complementary to the segmentation method and is called desegmentation method.

3.1 Green's function approach

Consider an N-port arbitrarily shaped planar circuit shown in Figure 3.1. The ports are located along the periphery and their widths are $w_i, w_j, \ldots$ etc. The rest of the periphery is an open boundary. Thus, the magnetic wall boundary condition ($\frac{\partial E_z}{\partial n} = 0$) holds. The excitation is done by coupling an external circuit to one of the ports of the planar circuit. The dimensions in x, y coordinates are comparable to the wavelength but, the substrate height normally is much smaller than the wavelength hence, one can assume that there is no variation of fields in the z-direction. That is, $\frac{\partial}{\partial z} = 0$ and $H_z = E_x = E_y = 0$, and the field components satisfy the two-dimensional Helmholtz wave equation. Therefore, for homogeneous and isotropic substrate the two-dimensional Helmholtz equation for E_z can be written as:

$$(\nabla_T^2 + k^2)E_z(x, y) = 0 \tag{3.1}$$

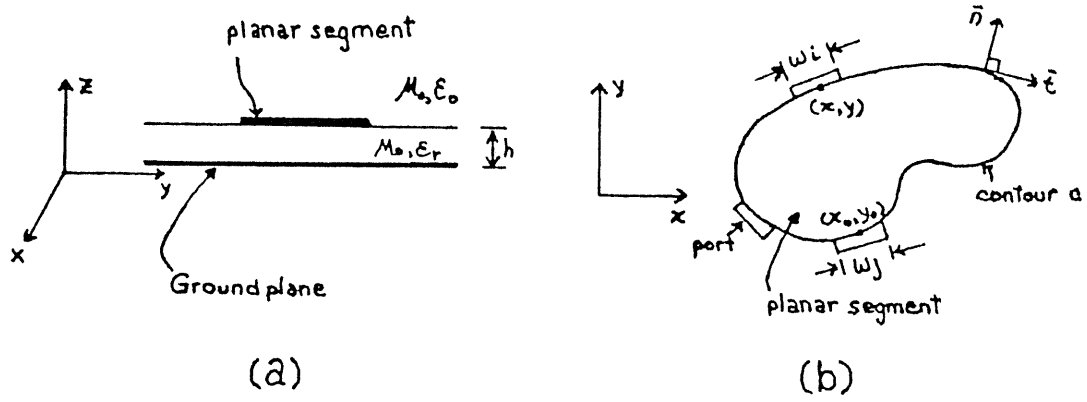

Figure 3.1: Microstrip type planar circuit: (a) side view; (b) top view of the planar segment.

where,

$$\nabla_T^2 = \frac{\partial^2}{\partial x^2} + \frac{\partial^2}{\partial y^2} \tag{3.2}$$

$$k = \omega\sqrt{\mu\epsilon} \tag{3.3}$$

The voltage for this two-dimensional component is related to the electric field E_z as:

$$v(x,y) = -hE_z(x,y) \tag{3.4}$$

where h represents the spacing between the planar conductor and the ground conductor (i.e. the substrate height). This voltage is related to a z-directed source current $i(x_0, y_0)$ by an impedance Green's function defined as:

$$v(x,y) = \int\int G(x,y \mid x_0, y_0)\, i(x_0, y_0) dx_0 dy_0 \tag{3.5}$$

The impedance Green's function $G(x,y \mid x_0, y_0)$ is the solution of:

$$(\nabla_T^2 + k^2) G(\bar{r} \mid \bar{r_0}) = -j\omega\mu h \delta(\bar{r} - \bar{r_0}) \tag{3.6}$$

where ∇_T^2 is defined by Equation (3.2); k is defined by Equation (3.3); and $\bar{r}$ represents the voltage point and $\bar{r_0}$ represents the source location.

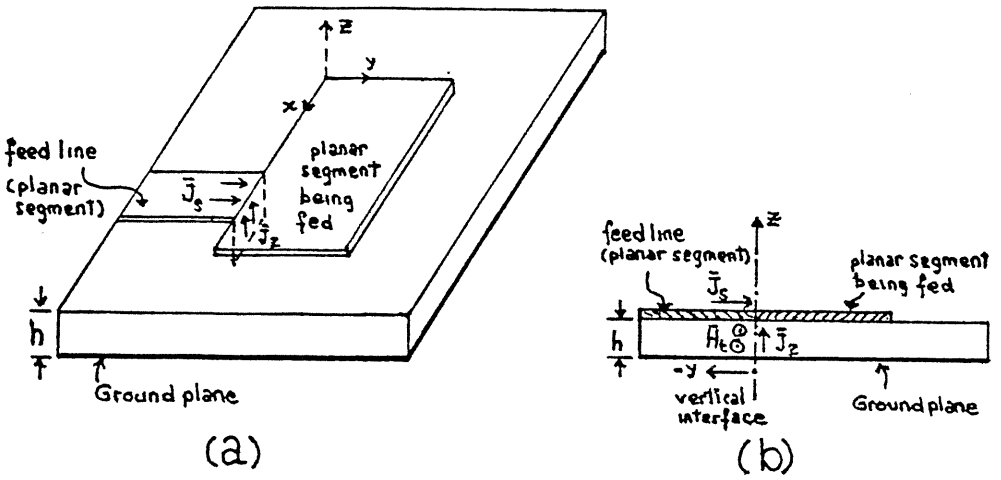

Figure 3.2: Equivalence between the port current and the z-directed current density at the junction between two planar circuits (the feed structure and the circuit being fed): (a) isometric view; (b) side view.

If the planar circuit is fed by another planar circuit as shown in Figure 3.2, the current flow $J_s(x_0, y_0)$ is in $x - y$ plane and not in the z-direction as assumed in the evaluation of the Green's function above. However, this feed current can be expressed in terms of an equivalent fictitious electric current density (z-directed) at the edge of the planar circuit being fed by considering the vertical interface between the two planar circuits (see Figure 3.2(b)).

The feed current can be expressed as $\bar{J}_s = \bar{y} \mid \bar{J}_s \mid$ and it is related to the magnetic field in the planar structure by $\bar{J}_s = \bar{n} \times \bar{H}$ where $\bar{n}$ underneath the strip is in $-z$-direction. The equivalent electric current density at the interface between the feed structure and the circuit being fed may now be expressed as:

$$\begin{aligned} \bar{J}_z &= \bar{n} \times \bar{H} \\ &= \bar{z} \mid \bar{H} \mid \end{aligned} \tag{3.7}$$

Since the feed current $\bar{J}_s = \bar{y} \mid \bar{J}_s \mid = -\bar{z} \times \bar{H}$ hence, using this in Equation (3.7) will give the following:

$$\bar{J}_z = \bar{z} \mid \bar{H} \mid = \bar{z} \mid \bar{J}_s \mid \tag{3.8}$$

Thus, $\bar{J}_s$ for a planar structure-fed port can be replaced by an equal magnitude of z-directed fictitious equivalent electric current density at the port location.

The equivalent z-directed current i_j fed at the j^{th} port of width w_j as shown in Figure 3.1 is given by:

$$i_j(x_0, y_0) = \int_{w_j} J_s(x_0, y_0) d\bar{r}_0 \tag{3.9}$$

where $J_s(x_0, y_0)$ is the input current over the port width w_j. Thus, from Equations (3.5), (3.6), and (3.9), and with the assumption that the current density are constant over the port widths w_i and w_j, the elements of the impedance matrix of the planar circuit can be expressed as:

$$Z_{ij} = \frac{1}{w_i w_j} \int_{w_i} \int_{w_j} G(x_i, y_i \mid x_j, y_j)\, d\bar{r}_i d\bar{r}_j \tag{3.10}$$

where $d\bar{r}_i$ and $d\bar{r}_j$ are the incremental distances over the port width w_i and w_j respectively.

The expressions for finding the impedance matrix elements of rectangular and three different triangular planar segments are given in the Appendix A.

3.2 Segmentation and Desegmentation methods

One of the methods used to analyze a more complex planar circuit (i.e. the circuit is made up of two or more regular segments) is known as segmentation method [1], [2], [3], [4], [5], [7]. A complementary procedure is known as desegmentation method [2], [3], [5], [6]. The segmentation and desegmentation methods using impedance matrices [1], [6] are discussed in this Section.

3.2.1 Segmentation method

Segmentation process involves breaking up a more complex planar circuit configuration into segments of regular shapes. Then, each segment is characterized by its impedance matrix. The combination of the impedance matrices of all the segments is used to evaluate the characterization of the whole circuit. To illustrate this segmentation process, consider the right-angle bend discontinuity shown in Figure 3.3. The discontinuity is broken up into two multiport segments (see Figure 3.3(b)). The impedance matrices for these

two segments are $[Z_A]$ and $[Z_B]$ respectively. The two segments are connected together by interconnected ports (q_i for segment A and r_i for segment B). The computational effort is reduced if q_1 is connected to r_1, q_2 to r_2,...etc. [1]. The external ports for each segment (p_a for segment A and p_b for segment B) are numbered first before the interconnection ports. The number of the external ports of segment A is p_a and that of segment B is p_b. There are q ($=r$) interconnected ports. The Z-matrices of both segments A and B can be written together as follow:

$$\begin{bmatrix} V_p \\ V_q \\ V_r \end{bmatrix} = \begin{bmatrix} Z_{pp} & Z_{pq} & Z_{pr} \\ Z_{qp} & Z_{qq} & Z_{qr} \\ Z_{rp} & Z_{rq} & Z_{rr} \end{bmatrix} \begin{bmatrix} I_p \\ I_q \\ I_r \end{bmatrix} \tag{3.11}$$

where $p = p_a + p_b$; V_p and I_p are the voltages and currents at the external ports p_a and p_b; and V_q, V_r and I_q, I_r are the voltages and currents at the interconnected ports q and r. The conditions for interconnecting q_i to r_i are:

$$V_q = V_r \tag{3.12}$$

and,

$$I_q + I_r = 0 \tag{3.13}$$

The Z-matrix of the overall configuration shown in Figure 3.3(a) can be computed by substituting Equations (3.12) and (3.13) into Equation (3.11) and eliminating V_q and I_r:

$$Z_c = Z_{pp} + (Z_{pq} - Z_{pr})(Z_{qq} + Z_{rr})^{-1}(Z_{rp} - Z_{qp}) \tag{3.14}$$

The voltages at the interconnected port, related to the currents flowing in the external ports p, can be computed by substituting Equations (3.12) and (3.13) into Equation (3.11) and eliminating V_p and I_r:

$$V_q = [Z_{qp} + Z_{qq}(Z_{qq} + Z_{rr})^{-1}(Z_{rp} - Z_{qp})]I_p \tag{3.15}$$

Finally, the Z-matrix can be converted into an S-matrix representation by the following relation:

$$S = \sqrt{Y_0}(Z_c - Z_0)(Z_c + Z_0)^{-1}\sqrt{Z_0} \tag{3.16}$$

where Z_0, $\sqrt{Z_0}$, and $\sqrt{Y_0}$ are diagonal matrices with the diagonal elements given by $Z_{01}, Z_{02}, \cdots, Z_{0n}$; $\sqrt{Z_{01}}, \sqrt{Z_{02}}, \cdots, \sqrt{Z_{0n}}$; and $\frac{1}{\sqrt{Z_{01}}}, \frac{1}{\sqrt{Z_{02}}}, \cdots, \frac{1}{\sqrt{Z_{0n}}}$ respectively. The diagonal matrix elements $Z_{01}, \cdots, Z_{0n}$ are the normalizing impedances at the various ports of the circuit.

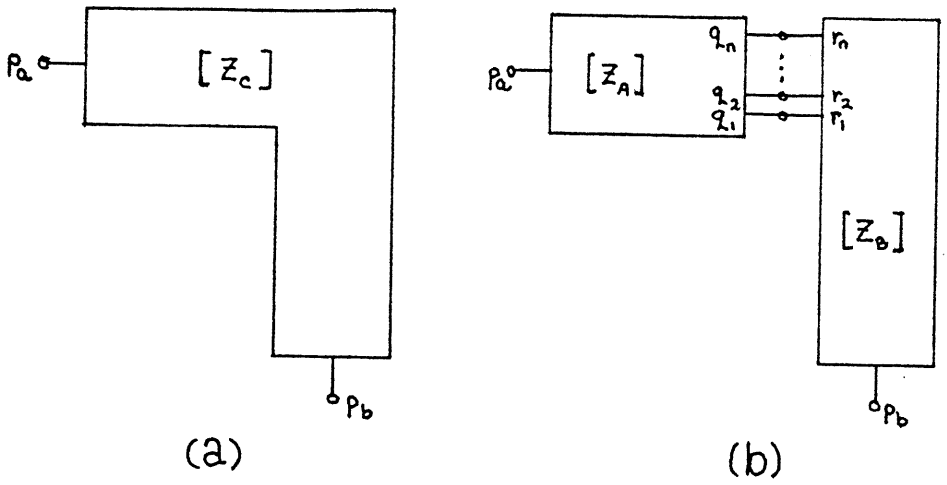

Figure 3.3: Right-angle bend discontinuity: (a) original/overall configuration; (b) the configuration is broken up into two multiport segments.

3.2.2 Desegmentation method

Desegmentation procedure is complementary to the segmentation method. It is used for two reasons: first, for analyzing circuit configurations which can not be solved by the segmentation method (see Figure 3.4); second, some circuit configurations are easier/simpler to analyze using desegmentation rather than segmentation method (see Figure 3.5). The desegmentation process involves adding a new segment/s to the original configuration. Then, the resulting new configuration and the added segment/s are characterized by their impedance matrices. The characterization of the original circuit is carried out by removing/de-embedding the impedance matrix of the added segment/s from the impedance matrix of the new configuration. To illustrate this desegmentation procedure, consider the chamfered right-angle bend discontinuity configuration shown in Figure 3.5(a,c).

If a triangular segment β is added to the original configuration α, the resulting new configuration γ is a right-angle bend which was analyzed in Section 3.2.1 (see also Figure 3.3). The impedance matrices for these two configurations are $[Z_\beta]$ and $[Z_\gamma]$ respectively. The two configurations are connected together by interconnected ports (q_i for configuration α and r_i

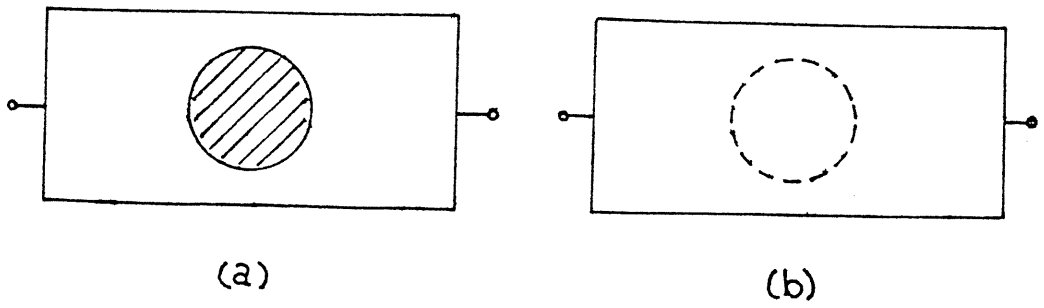

Figure 3.4: Circuit configuration for which desegmentation is needed: (a) original circuit; (b) a circular segment is added to perform the analysis.

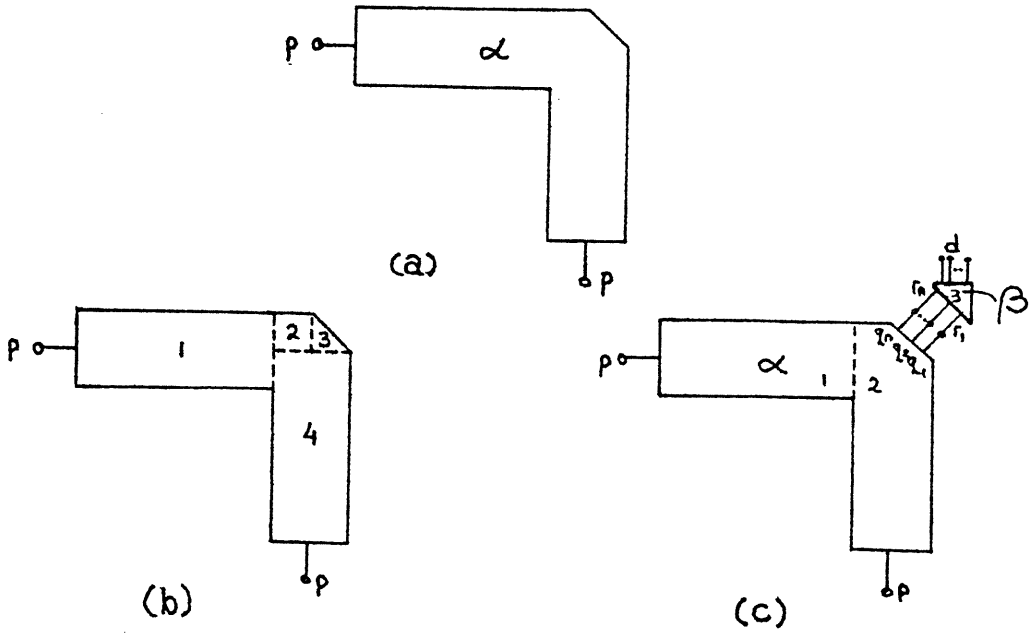

Figure 3.5: Chamfered right-angle bend discontinuity: (a) original circuit; (b) segmentation process involves analyzing four segments; (c) desegmentation process involves analyzing three segments only.

for configuration β). As in the segmentation process, q_1 is connected to r_1, q_2 to r_2,...etc. The d-ports are the external ports of segment β and the number of d-ports must be at least equal q or r. The p-ports are the external ports of segment α. Thus, the external ports of configuration γ are p and d. The conditions for interconnecting q_i to r_i are given by Equations (3.12) and (3.13). Therefore, the impedance matrix of the original configuration α, with $d = q = r$, can be expressed in terms of the impedance matrices of the β and γ configurations as:

$$Z^{\alpha}_{(p\times p)} = Z^{\gamma}_{pp} - Z_{pd}(Z^{\gamma}_{dd} - Z^{\beta}_{dd})^{-1} Z_{dp} \tag{3.17}$$

It may be noted that Equation (3.17) valid only for $d = q = r$. Thus, the scattering matrix of the original configuration (i.e. configuration α) can be determined using Equation (3.16) with Z_c replaced by Z^{α} found from above.

Chapter 4

Numerical Implementation

A computer program for implementation of planar analysis is discussed in the first Section of this Chapter. Then the three parameters that influence the convergence of the results are discussed next. In the last Section, a procedure for shifting the reference planes is described.

4.1 Planar circuit analysis program

A computer program for analyzing microstrip circuits/discontinuities has been developed. The formulas implemented in the computer program are those given in Chapter 2, Chapter 3, and in the Appendix A. A flowchart of the code implemented is provided in Figure 4.1. The input to the program can either be physical dimensions or line impedances. In both cases the effective parameters can then be computed from the formulas given in Chapter 2. Once the effective dimensions are obtained, then the configuration is broken up into multiport segments and the ports coordinates are computed. The impedance matrix of each segment is found by using the appropriate expression for a particular shape of the segment given in the Appendix A. The impedance matrix and the scattering matrix of the overall discontinuity configuration can then be determined from the formulas given in Section 3.2. Finally, the reference planes are shifted using the procedures outlined in Section 4.3.

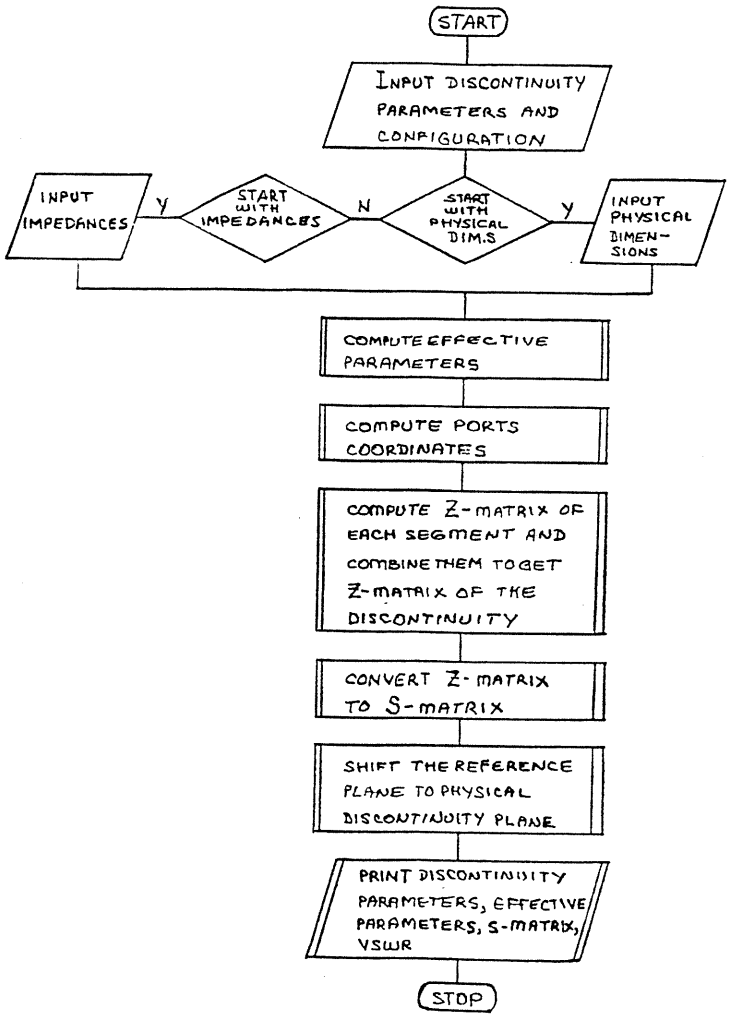

Figure 4.1: Flowchart of the Planar Circuit Analysis Program

4.2 Convergence of results

There are three parameters that influence the convergence, hence the accuracy, of the results:

- The number of terms used in computing the impedance matrix elements. The number of terms needed in the impedance matrix computation depends on the location and orientation of the ports involved in the computation. For the step-in-width discontinuity where all the ports are oriented in the same direction the number of terms needed is about ten as seen from Figure 4.2. However, larger number of terms are needed (about thirty) if the discontinuity analyzed is either right-angle bend or tee-junction. The number of terms needed is found by iterative computations. In the code developed 100 terms are used.

- The number of interconnected ports used in connecting two or more multi-port segments. The number of interconnected ports needed depends on the size of the segments involved. The values of $\mid S_{11} \mid$ obtained as a function of the number of interconnected ports in a symmetric step discontinuity is shown in Figure 4.3. From these results one can conclude that at least three interconnected ports are required. It might be noted that this result is valid only for one particular case. Again an iterative process is needed to find the optimum number of interconnected ports. In the code developed the number of interconnected ports is taken to be eight over the effective width of the line.

- The choice of reference plane for evaluating the impedance matrices. The choice of the reference plane means choosing the length of the segment that contains the external ports. There is a minimum length required for a segment in order to make sure that the higher order mode excited by the discontinuity decay to negligible value at the location of the external ports. In Figure 4.4, the value of $\mid S_{11} \mid$ for a symmetric step discontinuity is plotted as a function of the length of the wider segment normalized by its width. From the plot one can conclude that the length of the wider segment must be at least about 0.15 times its width. However, segment lengths of $\frac{\lambda}{4}$ and $\frac{\lambda}{2}$ are to be avoided in order to avoid any numerical error since $Z_{11} = Z_{22} \rightarrow 0$ for $\frac{\lambda}{4}$ segments and $Z_{11} = Z_{22} \rightarrow \infty$ for $\frac{\lambda}{2}$ segments.

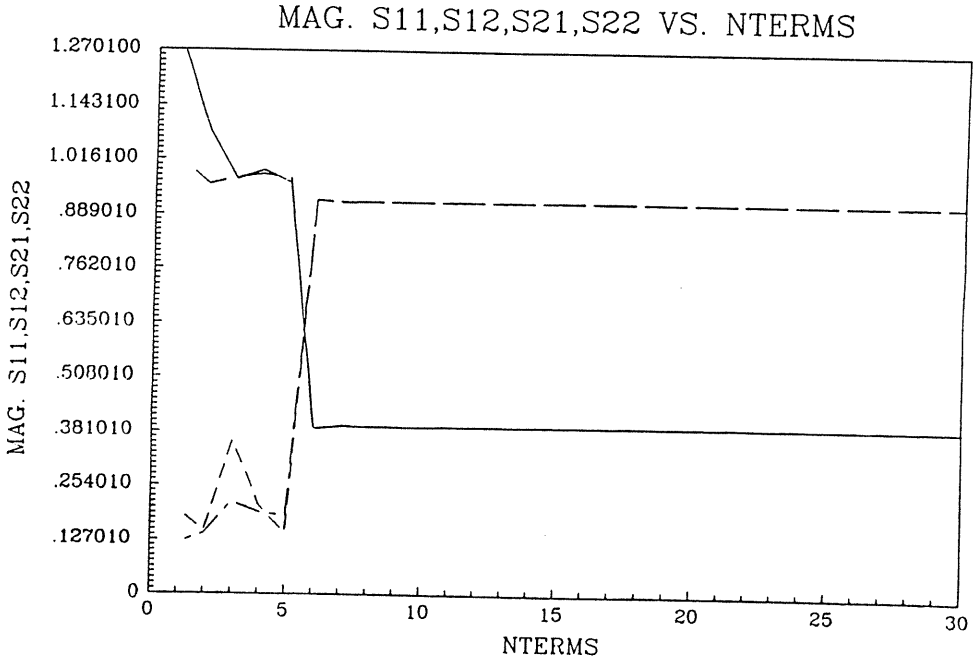

Figure 4.2: Variation of the number of terms ($NTERMS$) in step-in-width discontinuity analysis

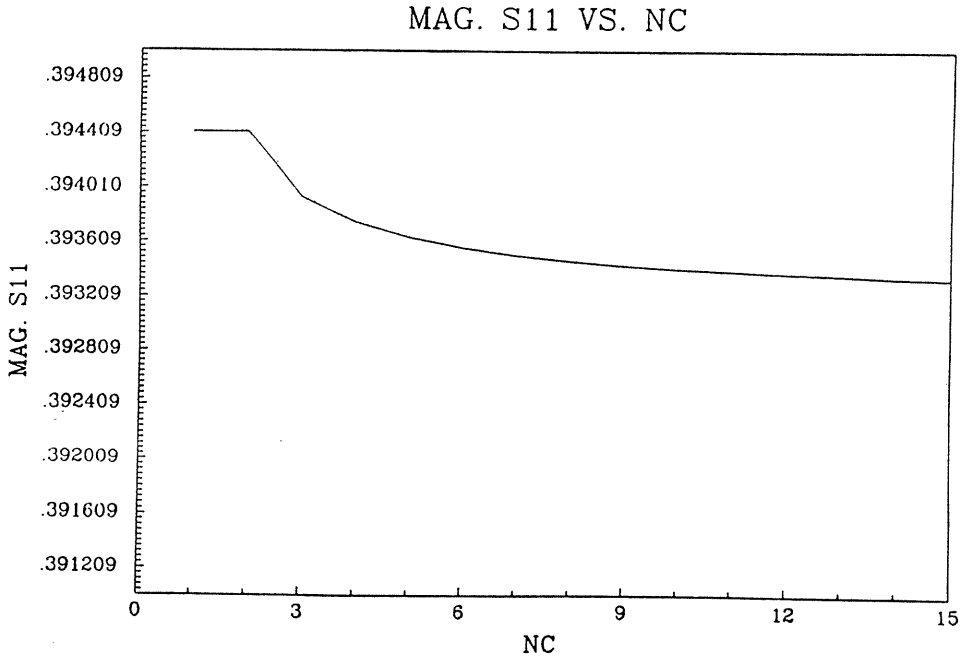

Figure 4.3: Variation of the number of interconnected ports (NC) in step-in-width discontinuity analysis

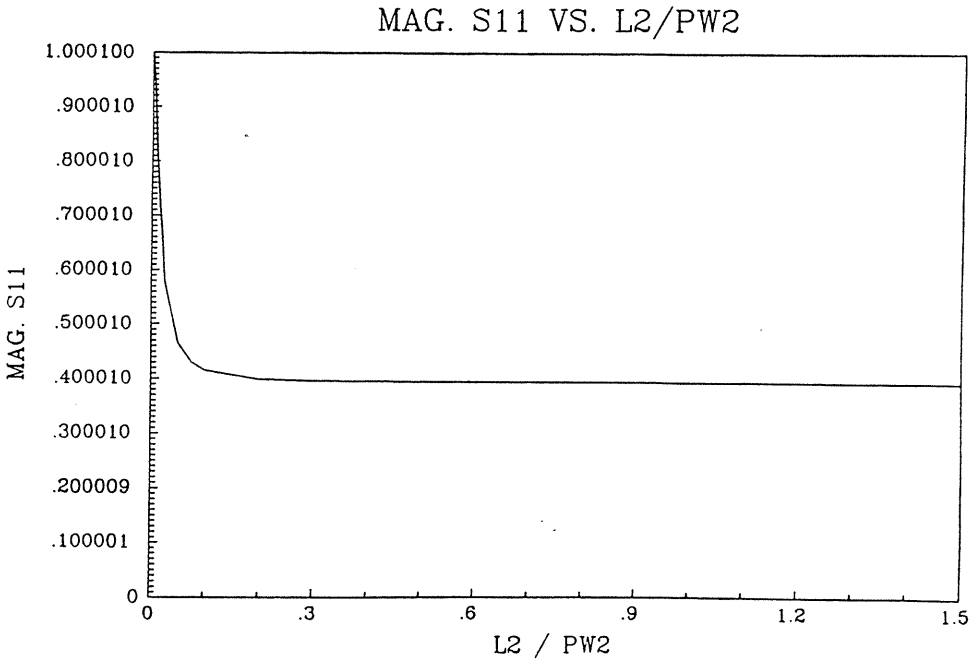

Figure 4.4: Variation of the length of the wider segment normalized by its width ($L2/W2$) in step-in-width discontinuity analysis

4.3 Shift of reference planes

In the analysis of microstrip discontinuities, the reference planes for specifying the scattering parameters are normally taken at the physical junction. However, the results obtained from segmentation and desegmentation methods are with respect to the reference planes at the edges containing the external ports of the discontinuity configuration. Thus, the reference planes given by these methods need to be shifted to the physical discontinuity planes. The situation for a 2-ports network is shown in Figure 4.5. For an N-ports network, the shift of the reference planes can be carried out as follows:

$$S'_{ii} = S_{ii} \exp(2\gamma_i L_i) \quad \text{for } i = 1, 2, \cdots, N \tag{4.1}$$

for $i = j$; and for $i \neq j$ the following is used:

$$S'_{ij} = S_{ij} \exp(\gamma_i L_i + \gamma_j L_j) \quad \text{for} \begin{cases} i = 1, 2, \cdots, N \\ j = 1, 2, \cdots, N \end{cases} \tag{4.2}$$

where S'_{ii} and S'_{ij} are the shifted $[S]$ matrix; S_{ii} and S_{ij} are the unshifted $[S]$ matrix; L_i and L_j are the lengths between the old and the new reference planes at external ports i and j respectively; and γ_i and γ_j are the complex propagation constant of the microstrip lines connected to the external ports i and j respectively. The propagation constant γ_i may be written as:

$$\begin{aligned} \gamma_i &= \alpha_i + \jmath\beta_i \\ &= \frac{\pi \tan\delta_e \sqrt{\epsilon_{r_{e_i}}(f)}}{\lambda_0} + \jmath \frac{2\pi f \sqrt{\epsilon_{r_{e_i}}(f)}}{c} \end{aligned} \tag{4.3}$$

for $i = 1, 2, \cdots, N$ and where $\tan\delta_e$ is the effective loss tangent as given by Equation (2.17); $\epsilon_{r_{e_i}}(f)$ is the effective dielectric constant at port i given by Equation (2.11); λ_0 is the free space wavelength; f is the operating frequency; and c is the speed of light ($= 3 \times 10^8$ meter/second).

Thus, using Equations (4.1) and (4.2) the reference plane of any N-ports networks/circuits can be located anywhere inside or outside the circuit. If L_i is positive then the reference plane is shifted inward (from the external port to the circuit inside). On the other hand, if L_i is negative then the reference plane is shifted outward (external to the circuit).

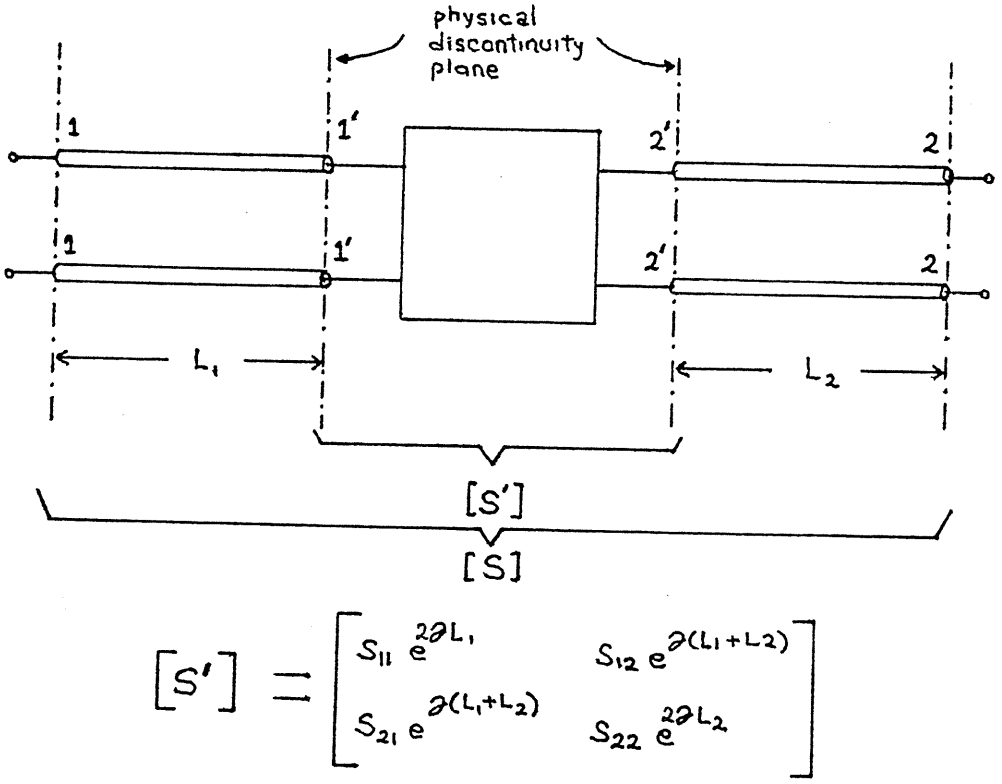

$$[S'] = \begin{bmatrix} S_{11}\, e^{2\gamma L_1} & S_{12}\, e^{\gamma(L_1+L_2)} \\ S_{21}\, e^{\gamma(L_1+L_2)} & S_{22}\, e^{2\gamma L_2} \end{bmatrix}$$

Figure 4.5: Shifting of reference plane in S-matrix for a 2-ports network

Chapter 5

Numerical Results

In this Chapter the results obtained using the planar analysis are compared to the results obtained by using other methods, namely quasi-static analysis and spectral domain analysis. The use of planar analysis for optimization of microstrip right-angle bend discontinuities are discussed and the results are compared with the results obtained by Chadha in [15] and Hammerstad in [16].

5.1 Comparison with quasi-static analysis

For this comparison a tee-junction discontinuity has been chosen. The parameters are chosen to be within the range of the quasi-static formula used which are given in [2]. The parameters used are given in Table 5.1 and the tee-junction configuration is shown in Figure 5.1.

The results for $\mid S_{11} \mid$, $\mid S_{12} \mid$, $\mid S_{13} \mid$, and $\mid S_{33} \mid$ obtained by the two methods are plotted in Figures 5.2-5.5 as a function of frequency (1 GHz to 18 GHz). The results show that at low frequency ($\sim 1 - 5GHz$) the

Table 5.1: Parameters for tee-junction discontinuity

Substrate height	25 mil
Strip thickness	0.7 mil
Dielectric constant	9.8
Loss tangent delta	0.001
Conductivity	5.8×10^7 mho/meter

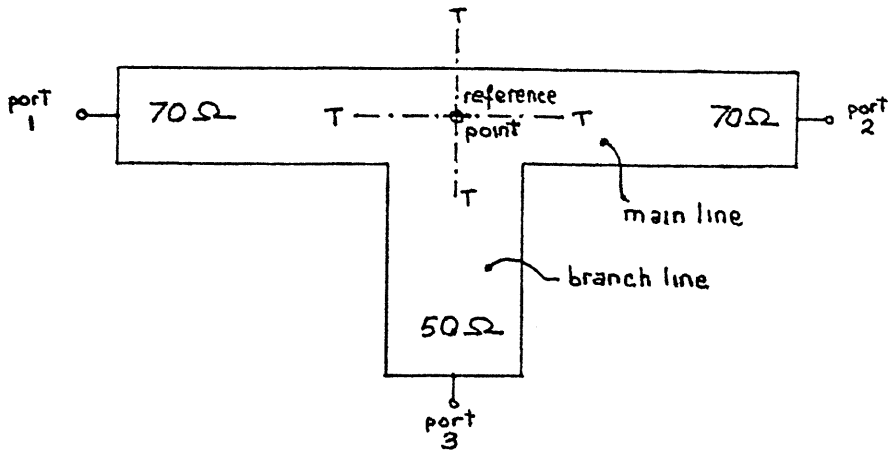

Figure 5.1: Tee-junction discontinuity configuration used for comparison with quasi-static analysis.

Table 5.2: Percent differences between planar and quasi-static analysis at 18 GHz.

Magnitude of	*Percent difference*
$S_{11} = S_{22}$	14.6
$S_{21} = S_{12}$	10.35
$S_{13} = S_{31} = S_{23} = S_{32}$	3.32
S_{33}	57.64

planar analysis results are relatively close to the quasi-static results. As the frequency increases the difference between these two results becomes more and more pronounced. This descrepancies at high frequencies are as expected since the quasi-static analysis does not account for the dispersion effect in microstrip discontinuities. The percent differences at 18 GHz are given in Table 5.2. Thus, one may conclude that in this case quasi-static results should not be used above about 5 GHz.

5.2 Comparison with spectral domain analysis

Koster and Jansen have done extensive analyses of microstrip step-in-width discontinuity (shown in Figure 5.6) using spectral domain method [17]. The

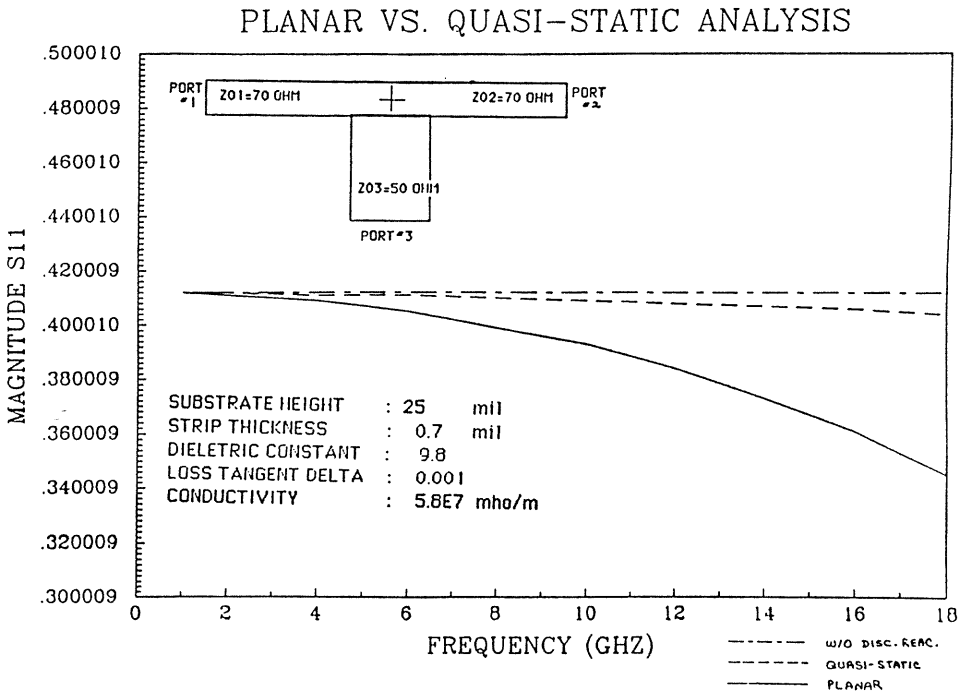

Figure 5.2: Planar analysis vs. quasi-static analysis for the reflections at the main line of the tee-junction.

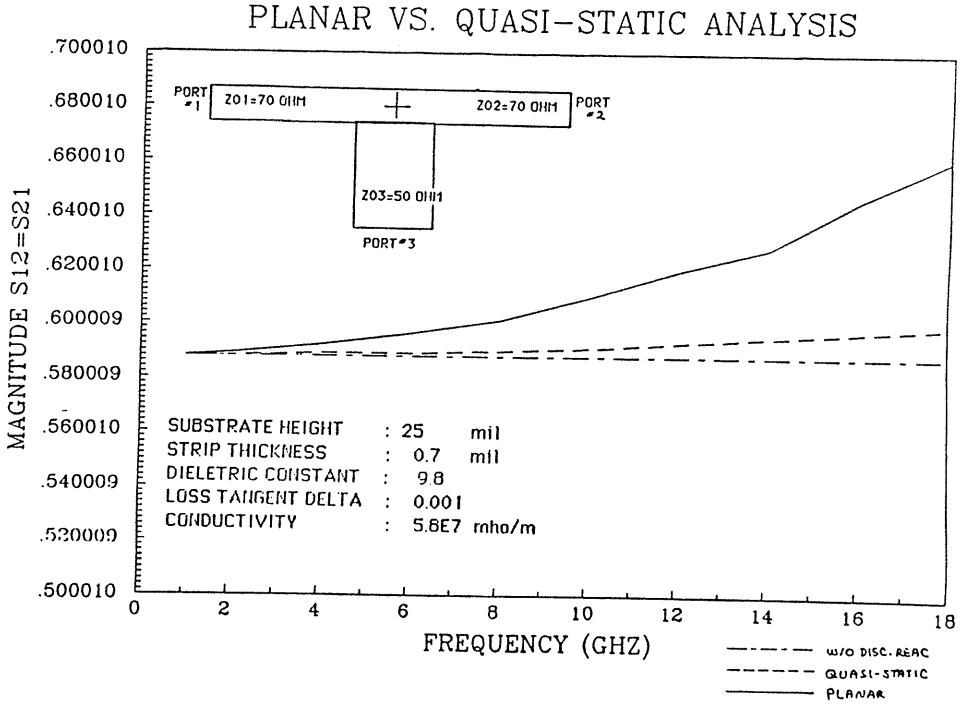

Figure 5.3: Planar analysis vs. quasi-static analysis for the transmissions at the main line of the tee-junction.

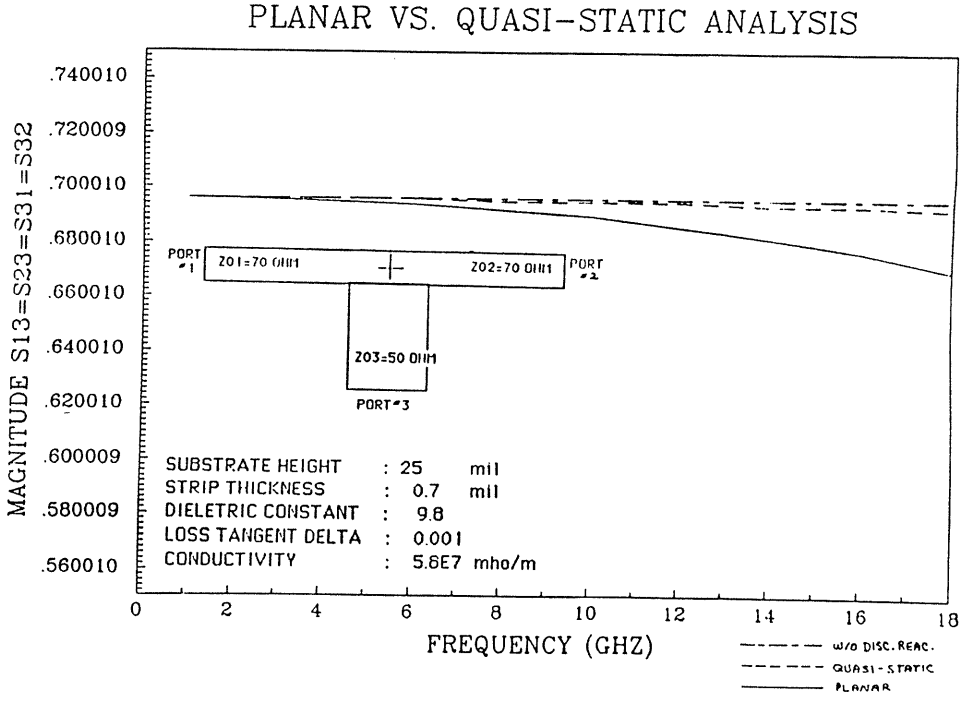

Figure 5.4: Planar analysis vs. quasi-static analysis for the transmissions between the main line and the branch line of the tee-junction.

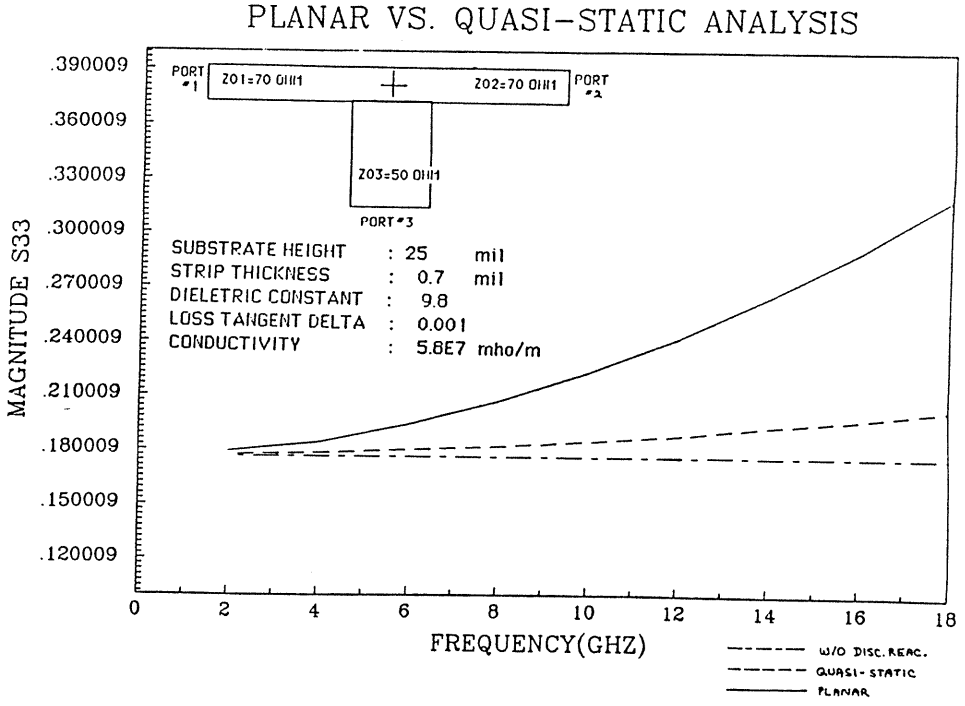

Figure 5.5: Planar analysis vs. quasi-static analysis for the reflection at the branch line of the tee-junction.

Table 5.3: Parameters for step-in-width discontinuity

Dielectric constant	2.32	10.0
Loss tangent delta	0.0009	0.0009
Substrate height	4.8×10^{-4} meter	6.0×10^{-4} meter
Strip thickness	1.778×10^{-5} meter	1.778×10^{-5} meter
Frequency	10.0 GHz	10.0 GHz

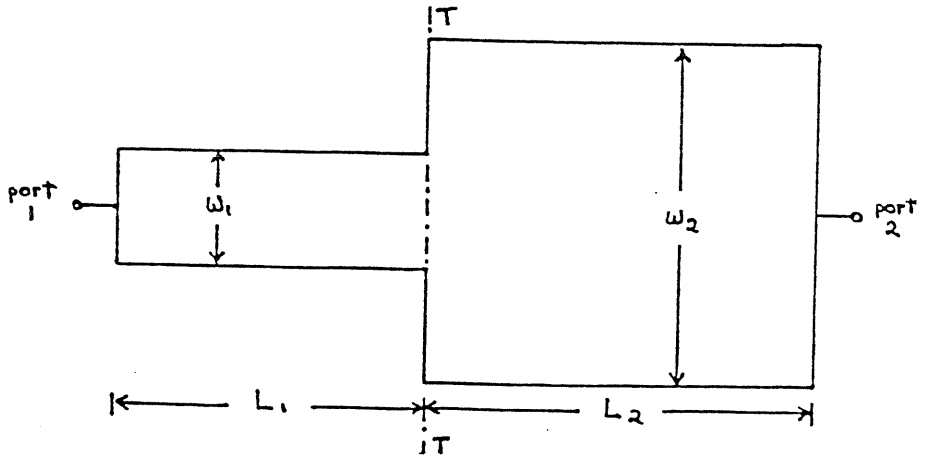

Figure 5.6: Step-in-width discontinuity configuration used for comparison with spectral domain analysis.

comparison between planar analysis and spectral domain analysis are carried out for low dielectric constant ($\epsilon_r = 2.32$) and for high dielectric constant ($\epsilon_r = 10$). The parameters chosen for these two cases are given in Table 5.3. This choice of parameters corresponds to $w_2/w_1 = 3$ and $d/\lambda_0 = 0.16$ for the low dielectric case ($\epsilon_r = 2.32$); and $w_2/w_1 = 3$ and $d/\lambda_0 = 0.02$ for the high dielectric case ($\epsilon_r = 10.0$) on the graphs given in [17], where d is the substrate height used in [17]. It may be noted that in this comparison $\frac{w_1}{h} = 5.4$ and $\frac{w_2}{h} = 11.8$ for the low dielectric case ($\epsilon_r = 2.32$); for the high dielectric case ($\epsilon_r = 10.0$) $\frac{w_1}{h} = 2.9$ and $\frac{w_2}{h} = 5.1$.

The comparison between planar analysis and spectral domain analysis is shown in Tables 5.4 and 5.5. The magnitudes of the reflected and transmitted wave given by planar analysis are in good agreement with those obtained by spectral domain analysis. The open end extension Δl (see Figure 2.3(c)) was taken to be zero in the planar analysis. Thus, the descrepancies in the phases

Table 5.4: Comparison between planar analysis and spectral domain analysis for low dielectric constant step-in-width discontinuity

$\epsilon_r = 2.32$			
Quantity	*Planar Analysis*	*Spectral domain Analysis*	*Percent Difference*
$\mid S_{11} \mid$	0.393	0.395	0.5
$\angle S_{11} deg.$	163.3	175.7	7.1
$\mid S_{12} \mid$	0.917	0.917	0.0
$\angle S_{12} deg.$	-4.7	-3.8	23.7
$\angle S_{22} deg.$	7.3	-3.3	95.9

Table 5.5: Comparison between planar analysis and spectral domain analysis for high dielectric constant step-in-width discontinuity

$\epsilon_r = 10.0$			
Quantity	*Planar Analysis*	*Spectral domain Analysis*	*Percent Difference*
$\mid S_{11} \mid$	0.310	0.314	1.3
$\angle S_{11} deg.$	165.3	175.7	5.9
$\mid S_{12} \mid$	0.945	0.944	0.1
$\angle S_{12} deg.$	-3.5	-4.2	16.7
$\angle S_{22} deg.$	7.8	-3.3	95.6

of the reflected and transmitted wave are large.

5.3 Optimization of right-angle bend microstrip discontinuity

Right-angle bend are used in microstrip circuit frequently. At the discontinuity section (i.e. at the bend) both the fields and the currents get disturbed. The current lines are concentrated at the inner corner, while at the outer corner there exists an extra fringing electric field. To eliminate/reduce this unwanted fringing fields, the outer corner of the bend is chamfered/mitred as shown in Figure 2.3(b). Thus, the compensation of right-angle bend discontinuities involves finding the optimum amount (percentage) of chamfering

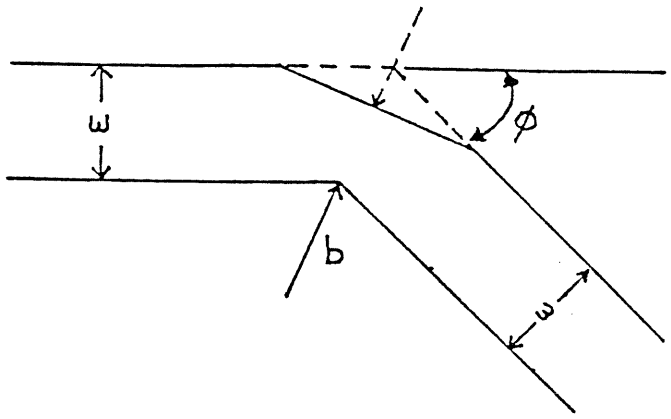

Figure 5.7: Definition of chamfering in microstrip bend discontinuity

needed to get zero or minimum reflection coefficient. In general, the percent chamfer for the bend shown in Figure 5.7 is defined as:

$$\% \; chamfer = (1 - \frac{b}{w}\cos(\frac{\phi}{2})) \times 100\% \tag{5.1}$$

For right-angle bend discontinuity, $\phi = 90°$, the $\% \; chamfer$ becomes:

$$\% \; chamfer = (1 - \frac{b}{w\sqrt{2}}) \times 100\% \tag{5.2}$$

In general, there are three criteria for determining an optimum discontinuity configuration:

- 1. minimum reflection (i.e. minimum $\mid S_{11} \mid$)
- 2. minimum variation of the equivalent electrical length with frequency
- 3. minimum radiation loss from the discontinuity

The planar analysis, reported here, allows one to satisfy the first and the second criteria. The equivalent electrical length Δl normalized by the substrate height can be computed as follows:

$$\frac{\Delta l}{h} = \frac{\phi_{12}}{\beta h} \tag{5.3}$$

where h is the substrate height; ϕ_{12} is the phase of the transmission coefficient (in *radians*); and $\beta = (2\pi f\sqrt{\epsilon_{r_e}(f)})/c$ is the propagation constant, with f is the operating frequency, $\epsilon_{r_e}(f)$ is the effective dielectric constant given by Equation (2.11).

The results of optimization of microstrip right-angle bend using planar analysis are compared with two other published results. The first one is based on the same method (i.e. planar analysis using segmentation method) [15]. The second one is the experimental results given by Hammerstad in [16].

5.3.1 Comparison with Chadha's results

Planar analysis of chamfered microstrip right-angle bend using segmentation method has been presented in [15]. The effective parameters of the chamfered right-angle bend analyzed are: dielectric constant = 6.781, width = 1.882 millimeter, and the substrate height = 0.65 millimeter. The comparison between the present results with those reported in [15] is shown in Figure 5.8.

The slight descrepancies between the two results are attributed to the fact that in the analysis performed in [15] the dielectric and conductor losses were not taken into account. Also, the formulas for computing the characteristic impedance and the effective dielectric constant used by [15] were not the same as those given in Chapter 2, i.e. the effect of dispersion was not taken into account in the analysis of [15]. Detailed computations show that the optimum chamfer is 41.4%.

5.3.2 Comparison with Hammerstad's Results

Hammerstad presented several experimental results for chamfered microstrip bends in [16]. For this comparison a 50Ω chamfered right-angle bend on a Rexolite substrate was chosen. The parameters of this right-angle bend are shown in Table 5.6.

The optimum chamfer for this right-angle bend according to [16] is 75%. In Figure 5.9, the magnitude of S_{11} is plotted as a function of the % $chamfer$. One can conclude that the optimum chamfer based on planar analysis is 56%. It may be noted that the values of $VSWR$ (obtained from the planar analysis) for % $chamfer$ of 75% and 56% are 1.340 and 1.003 respectively. The

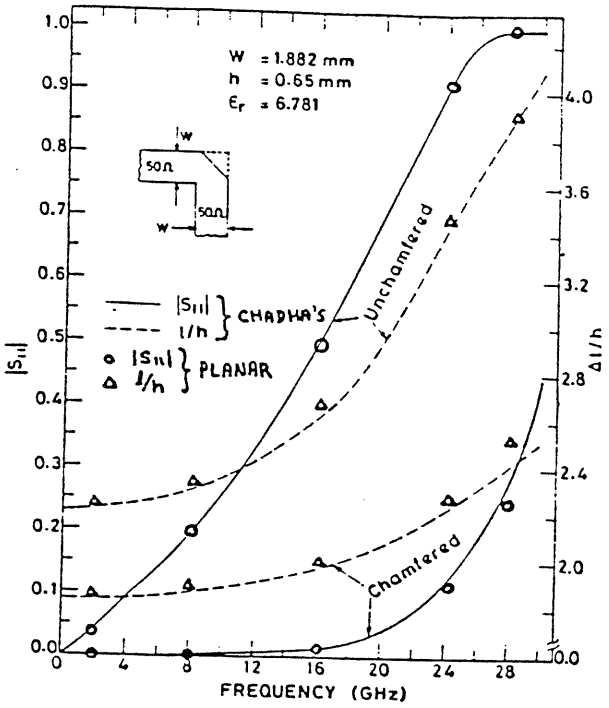

Figure 5.8: Comparison of the planar analysis results for chamfered microstrip right-angle bend with the results given by Chadha

Table 5.6: Parameters for chamfered right-angle bend

substrate height	3.175 millimeter
strip thickness	5 micron
dielectric constant	2.62
loss tangent delta	0.0001
conductivity	5.8×10^7 mho/meter
frequency	1.5 GHz

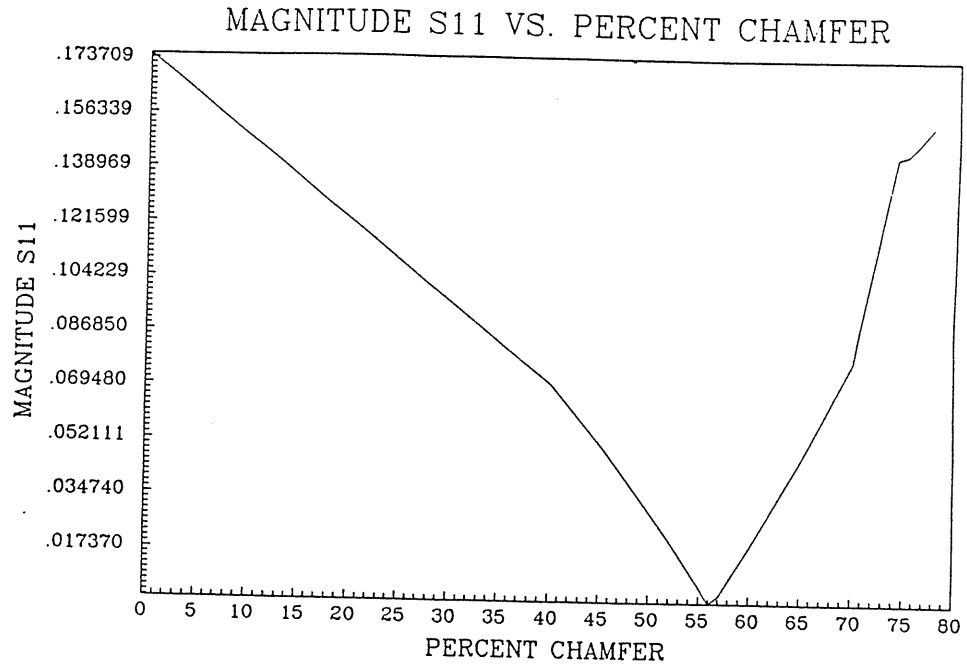

Figure 5.9: Optimum chamfer for microstrip right-angle bend

optimum chamfer given by planar analysis is lower than the optimum chamfer given by experimental results perhaps because of the fact that in the planar analysis the fringing field at the corner is not taken into account precisely. In the planar waveguide model of chamfered right-angle bend (see Figure 2.3(b)) the width extension taken at the discontinuity section (chamfered section) is less than the width extension for microstrip line section. These computation will be repeated with $\Delta C = (w_e(f) - w)/2$ (refer to Figure 2.3(b)).

Chapter 6

Concluding Remarks

The planar waveguide model for microstrip lines and the segmentation/desegmentation methods for planar circuit analysis have been used to develop a code for analysis of microstrip discontinuities (such as bends, steps, tee-junction, etc.). The criteria for convergence of results are discussed. The results for symmetric steps and tee-junctions have been compared with other results avilable in literatures. For the tee-junctions (on $\epsilon_r = 9.8$ and $h = 25$ mil substrate), the quasi-static results are found to be inaccurate above $5GHz$.

A comparison of the planar analysis results with full-wave analysis (spectral domain method) has also been carried out. At $10GHz$ (both for $\epsilon_r = 2.32$ and $\epsilon_r = 10.0$) agreement is better than 1.3%. It may be noted that for full-wave results reported in [17], the numerical accuracy claimed by the authors is about 1% because of convergence criteria used in their analysis. Also, the values for the results based on spectral domain analysis shown in Tables 5.4 and 5.5 are read from the graphs of [17]. This process itself can lead to about 2% error.

The results obtained for chamfered right-angle bend agree with those reported earlier by Chadha [15]. However, the value of the optimum chamfer (= 56%) obtained from planar analysis is somewhat different from the experimental result (= 75%) of Hammerstad [16]. As discussed earlier this is perhaps because of insufficient extension at the chamfered corner. A modified model of the chamfered corner is planned to be used in future work.

Three other possible configurations for the compensated bend are shown in Figure 6.1. These configurations will be analyzed and compared with the

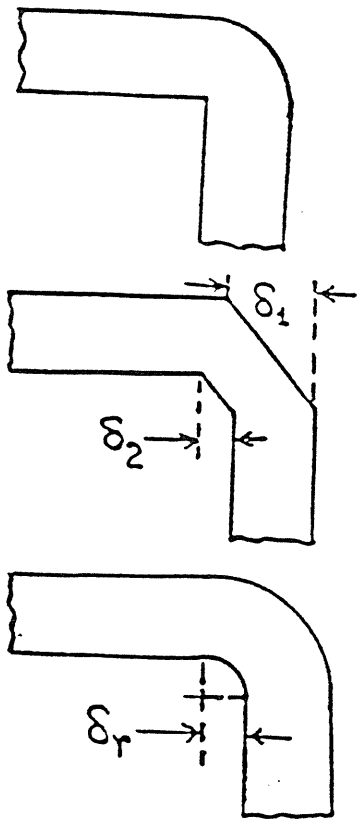

Figure 6.1: Three possible configurations for compensated microstrip right-angle bend.

simple truncated corner reported in Chapter 5.3.

Further work will also include compensation of tee-junction and step-junction discontinuity reactances. For the tee-junction, various geometries that needed to be compared for a compensated configurations are shown in Figure 6.2.

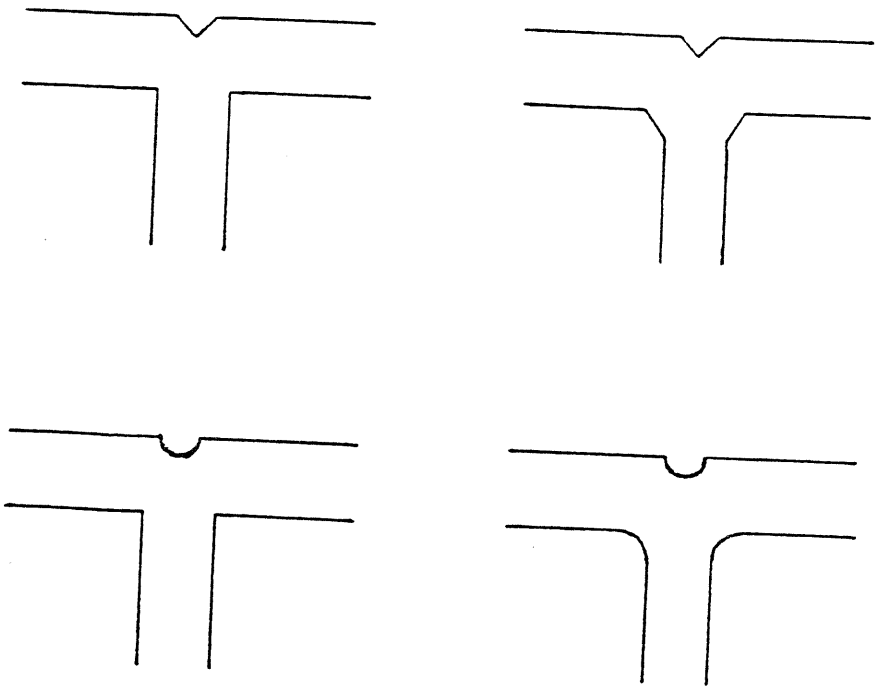

Figure 6.2: Compensated tee-junction configurations

Appendix A

Expressions for impedance matrix elements for rectangular and triangular segments

Knowing the Green's function of a particular configuration, the impedance matrix elements for the configuration can be computed using Equation (3.10). The impedance matrix elements for rectangular and triangular planar segments with open boundaries are presented in this Appendix A.

A.1 Z-matrix elements for a rectangular segment

In case of a rectangular segment the impedance matrix elements can be expressed in a single infinite series [18]. The geometry of the rectangular segment is specified in Figure A.1

A.1.1 Ports p and q are oriented in the same direction (x or y)

The Z-matrix elements Z_{pq} can be expressed as:

$$Z_{pq} = -CF\sum_{l=0}^{L}\sigma_l \cos(k_u u_p)\cos(k_u u_q)\cos(\gamma_l z_>)\cos(\gamma_l z_<)$$

$$\frac{sinc(\frac{k_u w_p}{2})sinc(\frac{k_u w_q}{2})}{\gamma_l \sin(\gamma_l F)} - \jmath C F \sum_{l=L+1}^{\infty} \cos(k_u u_q)\cos(k_u u_p)$$
$$sinc(\frac{k_u w_p}{2})sinc(\frac{k_u w_q}{2})\frac{\exp(-\jmath\gamma_l(v_> - v_<))}{\gamma_l} \tag{A.1}$$

where,

$$(v_>, v_<) = \begin{cases} (y_>, y_<) & for \;\; l = m \\ (x_>, x_<) & for \;\; l = n \end{cases} \tag{A.2}$$

$$C = \frac{\jmath\omega\mu_0 h}{ab} \tag{A.3}$$

$$F = \begin{cases} b & for \;\; l = m \\ a & for \;\; l = n \end{cases} \tag{A.4}$$

$$(u_p, u_q) = \begin{cases} (x_p, x_q) & for \;\; l = m \\ (y_p, y_q) & for \;\; l = n \end{cases} \tag{A.5}$$

$$\gamma_l = \pm\sqrt{k^2 - k_u^2} \tag{A.6}$$

$$k^2 = \omega^2\mu\epsilon_0\epsilon_r(1 - \jmath\delta_e) \tag{A.7}$$

here, δ_e is the effective loss tangent given by Equation (2.17).

$$k_u = \begin{cases} \frac{m\pi}{a} & for \;\; l = m \\ \frac{n\pi}{b} & for \;\; l = n \end{cases} \tag{A.8}$$

$$(z_>, z_<) = \begin{cases} (y_> - b, y_<) & for \;\; l = m \\ (x_> - a, x_<) & for \;\; l = n \end{cases} \tag{A.9}$$

$$y_> = max(y_p, y_q) \tag{A.10}$$

$$y_< = min(y_p, y_q) \tag{A.11}$$

$$x_> = max(x_p, x_q) \tag{A.12}$$

$$x_< = min(x_p, x_q) \tag{A.13}$$

$$\sigma_l = \begin{cases} 1 & for \;\; l = 0 \\ 2 & for \;\; l \neq 0 \end{cases} \tag{A.14}$$

If the ports p and q are oriented along x-direction then $l = m$ is chosen. On the other hand, if the ports p and q are oriented along y-direction $l = n$ is chosen. The sign of γ_l is chosen such that $\mathcal{I}m(\gamma_l)$ is negative. The integer L in Equation (A.1) is chosen so that $(\gamma_l F)$ is less than or equal to 50; this choice is a compromise between computational speed and accuracy.

A.1.2 Ports p and q are oriented in different directions

For this case, the Z-matrix elements can be expressed as:

$$\begin{aligned} Z_{pq} &= -CF\sum_{l=0}^{L}\sigma_l\cos(k_u u_p)\cos(k_u u_q)\cos(\gamma_l z_<)\cos(\gamma_l z_>) \\ &\quad \frac{sinc(\frac{k_u w_i}{2})sinc(\frac{\gamma_l w_j}{2})}{\gamma_l \sin(\gamma_l F)} - CF\sum_{l=L+1}^{\infty}\cos(k_u u_p)\cos(k_u u_q) \\ &\quad sinc(\frac{k_u w_i}{2})\frac{\exp(-j\gamma_l(v_> - v_< - \frac{w_j}{2}))}{\gamma_l^2 w_j} \end{aligned} \tag{A.15}$$

The integer l is chosen so that it satisfies the following condition:

$$(v_> - v_< - \frac{w_j}{2}) > 0 \tag{A.16}$$

Thus, the integer l is chosen according to the following conditions:

$$l = m \quad if \quad \{max(y_p, y_q) - min(y_p, y_q) - \frac{w_j}{2}\} > 0 \tag{A.17}$$

$$l = n \quad if \quad \{max(x_p, x_q) - min(x_p, x_q) - \frac{w_j}{2}\} > 0 \tag{A.18}$$

If $l = m$ then w_i corresponds to the port oriented in the x-direction and w_j corresponds to the port oriented in the y-direction. If $l = n$ then w_i corresponds to the port oriented in the y-direction and w_j corresponds to the port oriented in the x-direction. The notations given in Equations (A.2) to (A.14) are applicable in this case also.

A.2 Z-matrix elements for triangular segments

There are three different triangular configurations for which their Green's functions are available. The three triangular configurations are: right-angle isosceles triangle, 30° - 90° - 60° triangle, and equilateral triangle [19]. Thus, the impedance matrix elements for these three triangular configurations can be computed.

A.2.1 Z-matrix elements for a right-angle isosceles triangular segment

The geometry of the right-angle isosceles triangular segment is specified in Figure A.2.

The impedance matrix elements Z_{ij} can be expressed as:

$$Z_{ij} = \frac{j\omega\mu_0 h}{2} \sum_{m=0}^{\infty} \sum_{n=0}^{\infty} \frac{\sigma_m \sigma_n I_T(i) I_T(j)}{(m^2+n^2)\pi^2 - a^2 k^2} \tag{A.19}$$

where h is the substrate height; k^2 is given by Equation (A.7) and,

$$\sigma_m = \begin{cases} 1 & for \quad m = 0 \\ 2 & for \quad m \neq 0 \end{cases} \tag{A.20}$$

$$\sigma_n = \begin{cases} 1 & for \quad n = 0 \\ 2 & for \quad n \neq 0 \end{cases} \tag{A.21}$$

For ports located along the side OA:

$$\begin{aligned} I_T(i) &= \cos(k_x x_i) sinc(\frac{k_x w_i}{2}) \\ &\quad + (-1)^{m+n} \cos(k'_y x_i) sinc(\frac{k'_y w_i}{2}) \end{aligned} \tag{A.22}$$

For ports located along the side OB:

$$\begin{aligned} I_T(i) &= \cos(k'_y y_i) sinc(\frac{k'_y w_i}{2}) \\ &\quad + (-1)^{m+n} \cos(k_x y_i) sinc(\frac{k_x w_i}{2}) \end{aligned} \tag{A.23}$$

For ports located along the side AB:

$$\begin{aligned} I_T(i) &= (-1)^n \{\cos((k_x + k'_y)x_i) sinc((k_x + k'_y)\frac{w_i}{2\sqrt{2}}) \\ &\quad + \cos((k_x - k'_y)x_i) sinc((k_x - k'_y)\frac{w_i}{2\sqrt{2}})\} \end{aligned} \tag{A.24}$$

where,

$$k_x = \frac{m\pi}{a} \tag{A.25}$$

$$k'_y = \frac{n\pi}{a} \tag{A.26}$$

The Equations (A.22) to (A.26) can be applied to $I_T(j)$ by replacing the subscript i with j.

A.2.2 Z-matrix elements for a 30°-90°-60° triangular segment

The geometry of the 30°-90°-60° triangular segment is specified in Figure A.3.

The impedance matrix elements Z_{ij} can be expressed as:

$$Z_{ij} = 8\jmath\omega\mu_0 h \sum_{m=-\infty}^{\infty} \sum_{n=-\infty}^{\infty} \frac{I_{T_1}(i) I_{T_1}(j)}{16\sqrt{3}\pi^2(m^2+mn+n^2) - 9\sqrt{3}a^2k^2} \tag{A.27}$$

where h is the substrate thickness; k^2 is given by Equation (A.7). For ports located along the side OA:

$$\begin{aligned} I_{T_1}(i) &= (-1)^l \cos(\frac{2\pi l}{\sqrt{3}a} x_i) sinc(\frac{2\pi l}{\sqrt{3}a} \frac{w_i}{2}) \\ &+(-1)^m \cos(\frac{2\pi m}{\sqrt{3}a} x_i) sinc(\frac{2\pi m}{\sqrt{3}a} \frac{w_i}{2}) \\ &+(-1)^n \cos(\frac{2\pi n}{\sqrt{3}a} x_i) sinc(\frac{2\pi n}{\sqrt{3}a} \frac{w_i}{2}) \end{aligned} \tag{A.28}$$

For ports located along the side OB:

$$\begin{aligned} I_{T_1}(i) &= (-1)^l \cos(\frac{2\pi(m-n)}{3a} y_i) sinc(\frac{2\pi(m-n)}{3a} \frac{w_i}{2}) \\ &+(-1)^m \cos(\frac{2\pi(n-l)}{3a} y_i) sinc(\frac{2\pi(n-l)}{3a} \frac{w_i}{2}) \\ &+(-1)^n \cos(\frac{2\pi(l-m)}{3a} y_i) sinc(\frac{2\pi(l-m)}{3a} \frac{w_i}{2}) \end{aligned} \tag{A.29}$$

For ports located along the side AB:

$$\begin{aligned} I_{T_1}(i) &= \cos(\frac{4\pi(m-n)}{3a} y_i) sinc(\frac{4\pi(m-n)}{3a} \frac{w_i}{4}) \\ &\cos(\frac{4\pi(n-l)}{3a} y_i) sinc(\frac{4\pi(n-l)}{3a} \frac{w_i}{4}) \\ &\cos(\frac{4\pi(l-m)}{3a} y_i) sinc(\frac{4\pi(l-m)}{3a} \frac{w_i}{4}) \end{aligned} \tag{A.30}$$

The integers l, m, and n have to satisfy the following conditions:

$$l + m + n = 0 \tag{A.31}$$

The Equations (A.28) to (A.31) hold also for $I_{T_1}(j)$.

A.2.3 Z-matrix elements for an equilateral triangular segment

The geometry of the equilateral triangular segment is specified in Figure A.4.

The impedance matrix elements Z_{ij} can be expressed as:

$$Z_{ij} = 4j\omega\mu_0 h \sum_{m=-\infty}^{\infty} \sum_{n=-\infty}^{\infty} \frac{I_{T_1}(i)I_{T_1}(j) + I_{T_2}(i)I_{T_2}(j)}{16\sqrt{3}\pi^2(m^2+mn+n^2) - 9\sqrt{3}a^2k^2} \qquad \text{(A.32)}$$

where h is the substrate height and k^2 is given by Equation (A.7).

For ports located along the side BC the expressions for $I_{T_1}(i)$ and $I_{T_1}(j)$ are given by Equation (A.29). For ports located along the side AB or AC the expressions for $I_{T_1}(i)$ and $I_{T_1}(j)$ are given by Equation (A.30).

For ports located along the side BC:

$$\begin{aligned} I_{T_2}(i) \;=\; & (-1)^l \sin(\frac{2\pi(m-n)}{3a}y_i)sinc(\frac{2\pi(m-n)}{3a}\frac{w_i}{2}) \\ & +(-1)^m \sin(\frac{2\pi(n-l)}{3a}y_i)sinc(\frac{2\pi(n-l)}{3a}\frac{w_i}{2}) \\ & +(-1)^n \sin(\frac{2\pi(l-m)}{3a}y_i)sinc(\frac{2\pi(l-m)}{3a}\frac{w_i}{2}) \end{aligned} \qquad \text{(A.33)}$$

For ports located along the side AB or AC:

$$\begin{aligned} I_{T_2}(i) \;=\; & -\sin(\frac{4\pi(m-n)}{3a}y_i)sinc(\frac{4\pi(m-n)}{3a}\frac{w_i}{4}) \\ & -\sin(\frac{4\pi(n-l)}{3a}y_i)sinc(\frac{4\pi(n-l)}{3a}\frac{w_i}{4}) \\ & -\sin(\frac{4\pi(l-m)}{3a}y_i)sinc(\frac{4\pi(l-m)}{3a}\frac{w_i}{4}) \end{aligned} \qquad \text{(A.34)}$$

The Equations (A.33) and (A.34) hold also for $I_{T_2}(j)$. The integers l, m, and n have to satisfy the condition given in Equation (A.31).

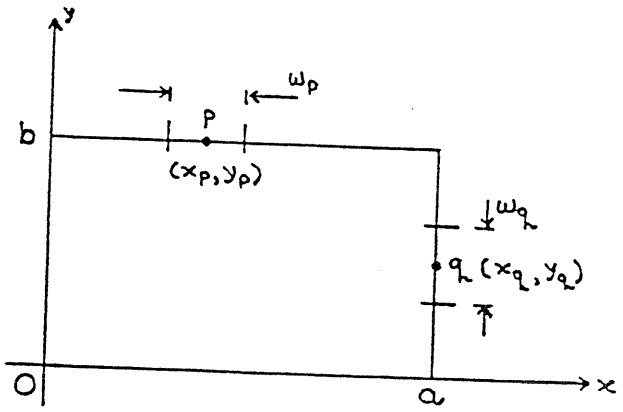

Figure A.1: Rectangular segment configuration and the ports locations

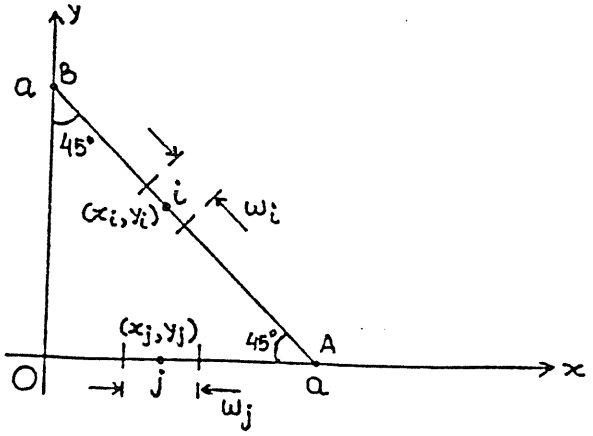

Figure A.2: Right-angle isosceles triangular segment configuration and the ports locations

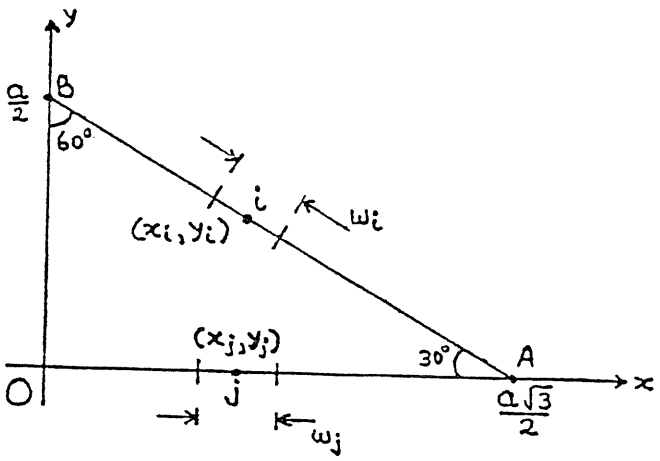

Figure A.3: 30°-90°-60° triangular segment configuration and the ports locations

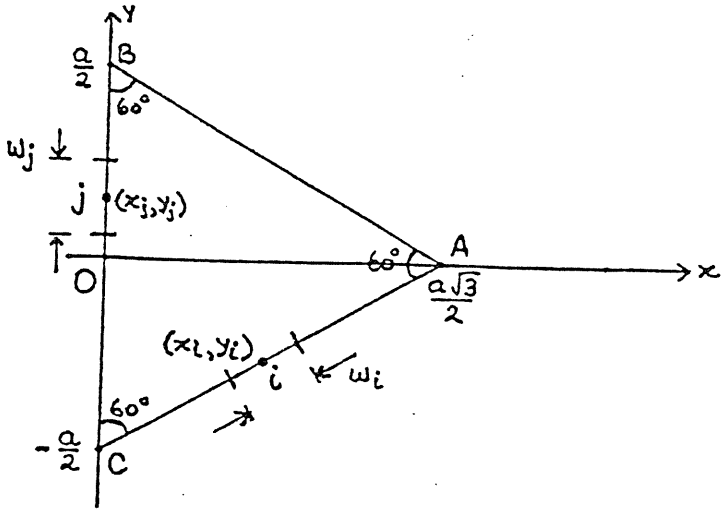

Figure A.4: Equilateral triangular segment configuration and the ports locations

Bibliography

[1] R. Chadha; K.C. Gupta: Segmentation method using impedance matrices for analysis of planar microwave circuits. *IEEE Trans. on Microwave Theory and Tech.*, Vol. MTT-29, Jan. 1981, pp. 71-74.

[2] K.C. Gupta; R. Garg; R. Chadha: Computer aided design of microwave circuits. *Artech House*, Massachusetts, 1981.

[3] K.C. Gupta: Two dimensional analysis of microstrip circuits and antennae. *Journal IETE*, Vol. 28, July 1982, pp. 346-364.

[4] T. Okoshi; Y. Uehara; T. Takeuchi: The segmentation method - an approach to the analysis of microwave planar circuits. *IEEE Trans. on Microwave Theory and Tech.*, Vol. MTT-24, Oct. 1976, pp. 662-668.

[5] T. Okoshi: Planar circuits for microwaves and lightwaves. *Springer-Verlag*, New York, 1985.

[6] P.C. Sharma; K.C. Gupta: Desegmentation method for analysis of two dimensional microwave circuits. *IEEE Trans. on Microwave Theory and Tech.*, Vol. MTT-29, Oct. 1981, pp. 1094-1098.

[7] R. Sorrentino: Planar circuits, waveguide models and segmentation method. *IEEE Trans. on Microwave Theory and Tech.*, Vol. MTT-33, Oct. 1985, pp. 1057-1066.

[8] R.K. Hoffmann: Handbook of microwave integrated circuits. *Artech House*, Massachusetts, 1987.

[9] G. Kompa; R. Mehran: Planar waveguide model for computing microstrip components. *Electronics Letters*, Vol. 11 No. 9, 1975, pp. 459-460.

[10] T. Okoshi; T. Miyoshi: The planar circuit - an approach to MIC. *IEEE Trans. on Microwave Theory and Tech.*, Vol. MTT-20, Apr. 1972, pp. 245-252.

[11] E.O. Hammerstad; O. Jensen: Accurate models for microstrip computer aided design. *IEEE MTT-S International Microwave Symposium Digest*, 1980, pp. 407-409.

[12] M.V. Schneider: Microstrip lines for microwave integrated circuits. *Bell System Technical Journal*, Vol. 48, May-June 1969, pp. 1421-1444.

[13] W.J. Getsinger: Microstrip dispersion model. *IEEE Trans. on Microwave Theory and Tech.*, Vol. MTT-21 No. 1, 1973, pp. 34-39.

[14] R.E. Collin: Field theory of guided waves. *Mc Graw Hill*, New York, 1960.

[15] R. Chadha; K.C. Gupta: Compensation of discontinuities in planar transmission lines. *IEEE Trans. on Microwave Theory and Tech.*, Vol. MTT-30, Dec. 1982, pp. 2151-2156.

[16] E.O. Hammerstad; F. Bekkadal: Microstrip handbook. *ELAB Report STF44 A74169*, Trondheim, Feb. 1975.

[17] N.H. Koster; R.H. Jansen: The microstrip step discontinuity: A revised description. *IEEE Trans. on Microwave Theory and Tech.*, Vol. MTT-34, Feb. 1986, pp. 213-223.

[18] A. Benalla; K.C. Gupta: Faster computation of Z-matrices for rectangular segments in planar microwave circuits. *IEEE Transaction on Mirowave Theory and Tech.*, Vol. MTT-34, June 1986, pp. 733-736.

[19] R. Chadha; K.C. Gupta: Green's functions for triangular segments in microwave planar circuits. *IEEE Trans. on Microwave Theory and Tech.*, Vol. MTT-20, Oct. 1980, pp. 1139-1143.